Supplement of Atmos. Chem. Phys., 18, 12613–12637, 2018
https://doi.org/10.5194/acp-18-12613-2018-supplement

Atmospheric Chemistry and Physics
Open Access
EGU

Supplement of

Experimental and model estimates of the contributions from biogenic monoterpenes and sesquiterpenes to secondary organic aerosol in the southeastern United States

Lu Xu et al.

Correspondence to: Nga Lee Ng (ng@chbe.gatech.edu)

S1. Experimental Procedure

The perturbation experiments were performed in July-August 2016. A $2m^3$ Teflon chamber (cubic shape) (Fig. 1) was placed outdoor on the rooftop of the Environmental Science and Technology (ES&T) building on the Georgia Institute of Technology (GT) campus, which is 30-40m above the ground and 840m away from interstate I75/85. The eight corners of the chamber were open (~2"×2") to the atmosphere to allow for continuous exchange of air with the atmosphere. All analytical instruments were placed inside the building, which is about 4-5m away from the chamber. The instruments were connected to the chamber using 1/4" teflon tubings (for measurements of gas-phase species) or stainless steel tubings (for measurement of particle-phase species). The sampling inlets were inserted into the center of the chamber.

The perturbation procedure is described below and illustrated in Fig. A1. Firstly, we continuously flushed the chamber with ambient air using two fans, which were placed at two corners of the chamber. During this flushing period, all instruments sampled ambient air and were not connected to the chamber. The flushing period lasted at least 3 hours to ensure that the air composition in the chamber is the same as ambient composition. Secondly, we stopped both fans and connected all instruments to chamber. Due to particle wall loss in the chamber, the particle mass concentration in the chamber was lower than that in the atmosphere (Fig. A1), but the particle composition in the chamber was almost the same as that in the atmosphere (Fig. S10), because the particle wall loss mainly depends on particle size not particle composition (Keywood et al., 2004). Due to the continued sampling by the instruments (~20 liter per minute, LPM) and the open corners of the chamber, ambient air continuously entered the chamber, even the two fans were turned off during this period. The main reason to turn off the fans is to increase the residence time of species in the chamber. The main reasons to leave the eight corners of chamber open are (a) to supply the chamber with atmospheric oxidants and (b) ensure that air composition in the chamber is representative of ambient composition. Thirdly, after sampling the chamber for about 30min, we injected certain amount of VOC (liquid) into the chamber with a needle, which vaporized upon injection. We continuously monitored the chamber composition for ~40 min after VOC injection. Lastly, we disconnected all instruments from the chamber, sampled ambient air, and turned on two fans to flush the chamber to prepare for the next perturbation experiment. In brief, one perturbation experiment can be divided into the following four periods: Amb_Bf (30min ambient measurement period before sampling chamber), Chamber_Bf (from sampling chamber to VOC injection, a

period ~30min), Chamber_Af (from VOC injection to stop sampling chamber, a period ~40min), and Amb_Af (30min ambient measurement period after sampling chamber).

One to three experiments were performed per day. The interval between two experiments was at least 3 hours, which avoids the interference of chamber content from previous experiments. The perturbations were performed at different times of day to probe aerosol formation under different reaction conditions. 0.2 μL α-pinene or β-caryophyllene was injected via a needle into the chamber. This provides initial concentrations of α-pinene and β-caryophyllene to be 14ppb and10ppb in the chamber, respectively, assuming they are well mixed in the $2m^3$ chamber. For isoprene and *m*-xylene perturbation experiments, we tried a range of initial VOC concentrations (i.e., 10-90ppb for isoprene and 10-540ppb for *m*-xylene). For naphthalene perturbation experiments, we injected naphthalene by passing pure air over solid naphthalene flakes. We did not observe OA formation from these three VOCs, regardless of VOC concentration. The possible reasons of the lack of OA formation will be discussed in section S6. Due to no OA formation, the details about perturbation experiments with isoprene, *m*-xylene, and naphthalene are not included in Table S4.

In this study, we selected α-pinene and β-caryophyllene as representatives of monoterpenes and sesquiterpenes due to the following reasons. Firstly, both VOCs are widely studied in the literature. Secondly, they are the most abundant species in monoterpenes and sesquiterpenes, respectively (Guenther et al., 2012; Helmig et al., 2007). Thirdly, the mass spectra of SOA from VOCs in the same class generally share similar features. For example, the correlation coefficient (i.e., R) between the mass spectra of SOA from the β-caryophyllene and α-humulene is 0.97 (Bahreini et al., 2005). Still using the mass spectra reported in Bahreini et al. (2005), the R between α-pinene SOA and other monoterpenes SOA (β-pinene, α-terpinene, myrcene, and terpinolene) is larger than 0.9. Fourthly, in addition to the similar mass spectra, the time series of α-pinene in the southeastern U.S. is similar to that of other monoterpenes, such as β-pinene and camphene (Xu et al., 2015a). Further studies with other monoterpenes and sesquiterpenes are still required to confirm the representativeness of α-pinene and β-caryophyllene.

In the perturbation experiments, we aimed to produce small amount of SOA, which would not substantially perturb the composition of existing organic aerosol. The difference in OA concentration between "Chamber_Bf" and "Chamber_Af" is within 4 μg m^{-3} (Fig. S11) and the

OA mass spectrum in Chamber_Af is almost identical to that in Chamber_Bf (Fig. S12). In the α-pinene and β-caryophyllene experiments, the concentrations of inorganic species, including SO_4, NO_3, and NH_4, during "Chamber_Bf" and "Chamber_Af" are shown in Fig. S11.

S2. High Resolution Time-of-Flight Aerosol Mass Spectrometer (HR-ToF-AMS)

The HR-ToF-AMS measures the chemical composition and size distribution of submicron non-refractory species ($NR\text{-}PM_1$) with high temporal resolution. The details about HR-ToF-AMS principles have been extensively discussed in the literature(Canagaratna et al., 2007; DeCarlo et al., 2006). In brief, HR-ToF-AMS samples particles through an aerodynamic lens and then impacts the particles on a ~600°C tungsten surface. Non-refractory species are flash evaporated and the resultant vapors are ionized by 70eV electron impact ionization. The generated ions are analyzed using time-of-flight mass spectrometry. In this study, the temporal resolution of HR-ToF-AMS measurements was set to be 2 minutes and the instrument was only operated in V mode (resolving power ~2100 at *m/z* 200). Ambient filter measurements (with a HEPA filter placed at the inlet of sampling line) were performed periodically to eliminate gas-phase interference on the particle-phase measurements by the HR-ToF-AMS. Ionization efficiency (IE) calibrations were conducted every week with 300nm ammonium nitrate (AN) particles. A nafion dryer was placed upstream of the HR-ToF-AMS to dry particles (relative humidity < 20%), which eliminated the potential effect of relative humidity on particle collection efficiency (CE) at the HR-ToF-AMS vaporizer(Matthew et al., 2008). The composition-dependent CE (i.e., CDCE) was applied to the data, based on the algorithm proposed by Middlebrook et al.(Middlebrook et al., 2012) The elemental ratios, such as atomic O:C and H:C, were calculated based on the method in Canagaratna et al.(Canagaratna et al., 2015) The data analysis was performed using the standard AMS analysis toolkits SQUIRREL v1.57H and PIKA v1.16H in Igor Pro 6.36 (WaveMetrics Inc.).

S3. Positive Matrix Factorization (PMF) Analysis

Positive Matrix Factorization (PMF) analysis has been widely used for aerosol source apportionment in the atmospheric chemistry community(Jimenez et al., 2009; Crippa et al., 2014; Xu et al., 2015a). PMF solves bilinear unmixing factor model(Paatero and Tapper, 1994; Ulbrich et al., 2009b)

$$X = TS \times MS + E \qquad \text{Eqn 2}$$

X is an $m \times n$ matrix, representing m measurements over time of n species (i.e., m/z in AMS measurements). TS is an $m \times p$ matrix, representing the factor strength (i.e., concentration in AMS measurements) of the p factors. MS is an $p \times n$ matrix, representing the source profile (i.e., mass spectra in AMS measurements) of the p factors. E is an $m \times n$ matrix, representing the unexplained residual by the p factors. PMF solves the equation by minimizing the summed least squares errors of the fit weighted with the error estimates of each measurement. In other words, PMF represents the observed organic mass spectra as a linear combination of a number of factors with constant mass spectra but varying concentrations over time. PMF groups OA constituents with similar mass spectra and temporal variation into different factors, which are related to characteristic sources and atmospheric processes.

In this study, we performed PMF analysis on the high-resolution mass spectra of organic species (inorganic species are excluded) of combined ambient and perturbation data. Each OA factor has a constant mass spectrum throughout the study, regardless of ambient or chamber periods. The organic data matrix and error matrix were generated from PIKA v1.16H and processed in the PMF Evaluation Toolkit (PET) software or Solution Finder (SoFi) software(Ulbrich et al., 2009b). *m/z*'s with signal-to-noise ratio between 0.2 and 2 were downweighted by a factor of 2 to reduce disproportionate effects on the results (Ulbrich et al., 2009a). We do not observe *m/z*'s with signal-to-noise ratio smaller than 0.2. The errors of all CO_2^+ related peaks (i.e., O^+, HO^+, H_2O^+, CO^+, and CO_2^+) were downweighted, to avoid excessive weighting of CO_2^+. The error of CHO^+ (*m/z* 29.0027) was downweighted by a factor of 2 as its error appears to be underestimated, possibly due to interference from its adjacent N_2 isotope ion (*m/z* 29.0032). We utilized the PMF2 solver, which does not require a priori information and reduces subjectivity. We performed 100 bootstrapping runs to quantify the uncertainty of PMF results.

Fig. 2 shows the time series and mass spectra of OA factors resolved in the measurements. Five OA factors (i.e., HOA, COA, isoprene-OA, LO-OOA, and MO-OOA) are resolved. PMF solutions with more than five OA factors display splitting behavior of existing factors instead of providing new factors. Also, we note that PMF solutions with more OA factors cannot resolve one factor that is capable of representing all perturbation induced SOA. The five identified OA factors

have been extensively discussed in previous studies (Xu et al., 2015a; Xu et al., 2015b; Xu et al., 2017). Below, we describe the unique features of these OA factors.

The mass spectrum of hydrocarbon-like OA (HOA) is dominated by hydrocarbon-like ions ($C_xH_y^+$ ions), which is similar to that of primary combustion emission species (Zhang et al., 2011). The time series of HOA correlates well with primary emissions (i.e., black carbon and NO_x). Thus, HOA is a surrogate of primary OA from vehicle emissions (Zhang et al., 2011).

The mass spectrum of cooking OA (COA) is characterized by prominent signal at ions $C_3H_5^+$ (*m/z* 41) and $C_4H_7^+$ (*m/z* 55), which is similar to the mass spectrum of unsaturated fatty acids (Huang et al., 2010; Mohr et al., 2009). Cooking is an important source of primary emission in urban sites(Xu et al., 2015a; Crippa et al., 2014; Huang et al., 2010), the concentration of which is even higher than HOA concentration sometimes (Huang et al., 2010). We have clear evidence that the COA factor at the measurement site has contributions from cooking activities. Firstly, the diurnal variation of COA peaks during meal times (Fig. S6a). Secondly, in another dataset from the same measurement site, the COA concentration shows clear increases on football days, consistent with barbecue activities on campus and close to the measurement site. Thirdly, compared to most of days during 2015 measurement (section S4), the COA concentration is higher between August 13th and 16th, 2015 (Fig. S6b and S6c). These four days are right before the start of a new semester and thus there are many fraternity rush events (i.e., barbecue activities) on campus. However, the COA concentration increases in 5 out of 6 β-caryophyllene perturbation experiments and its enhancement amount is ~25% of LO-OOA enhancement (Fig. S5b), which shows that COA factor could have interference from β-caryophyllene SOA. Thus, caution is required when using COA factor as a surrogate for cooking emissions, especially for urban sites influenced by air masses from forested areas.

Ample evidence suggests that the isoprene-derived OA (isoprene-OA) factor is related to the reactive uptake of isoprene oxidation products, isoprene epoxydiols (IEPOX) (Xu et al., 2015a; Lin et al., 2012; de Sá et al., 2016). Firstly, the mass spectrum of isoprene-OA is characterized by prominent signal at ions $C_4H_5^+$ (*m/z* 53) and $C_5H_6O^+$ (*m/z* 82), which is similar to the mass spectrum of laboratory IEPOX SOA (Lin et al., 2012). Secondly, the time series of this factor correlates well with 2-methyltrols, which are tracers for isoprene SOA tracers and likely formed from the reactive uptake of IEPOX. This factor is also referred to as "IEPOX-OA" in some studies (Hu et al., 2015;

Budisulistiorini et al., 2013; Budisulistiorini et al., 2015; de Sá et al., 2017). The isoprene-OA factor contributes 18-36%, 34%, and 24% of OA in the southeastern U.S. (Xu et al., 2015a), Amazonia forest (Chen et al., 2015), and boreal forest (Robinson et al., 2011). Our perturbation experiments point out the possibility that isoprene-OA factor could have interference from α-pinene SOA. From another aspect, the enhancement in isoprene-OA in these experiments suggests that fresh α-pinene SOA is not exclusively apportioned to LO-OOA, at least for the sites with isoprene-OA.

Less-oxidized oxygenated organic aerosol (LO-OOA) and more-oxidized oxygenated organic aerosol (MO-OOA) are named based on their differing carbon oxidation state. MO-OOA has the highest atomic O:C ratio, indicating that it is highly oxidized. LO-OOA has lower O:C ratio than MO-OOA. In the southeastern U.S., MO-OOA concentration peaks in the afternoon and LO-OOA exhibits a daily maximum at night (Xu et al., 2015b).

We examined the PMF residual (i.e., Q/Q_{exp}) in α-pinene and β-caryophyllene perturbation experiments. As shown in Fig. S13a, in α-pinene experiments, the difference in Q/Q_{exp} between "Chamber_Bf" (before α-pinene injection) and "Chamber_Af" (after α-pinene injection) is not statistically significant. This suggests that PMF analysis has adequately accounted for the newly formed α-pinene SOA. In contrast, in β-caryophyllene experiments, there is a clear pattern that Q/Q_{exp} in "Chamber_Af" is larger than that in "Chamber_Bf" (Fig. S13b). This likely arises from the rapid change in the subtleties of OA composition caused by the newly formed β-caryophyllene SOA. The larger Q/Q_{exp} in β-caryophyllene experiments than α-pinene experiments may be a result of that ΔOA (i.e., the difference in OA concentration between "Chamber_Af" and "Chamber_Bf") is larger in β-caryophyllene experiments (average value 1.95 μg m^{-3} over 6 experiments) than α-pinene experiments (average value 0.98 μg m^{-3} over 14 experiments). The behavior of Q/Q_{exp} is not quite expected because the OA mass spectra after injecting β-caryophyllene are almost identical to those before perturbation (i.e., R between Chamber_Bf and Chamber_Af is >0.99 as shown in Fig. S12b). The larger Q/Q_{exp} in Chamber_Af likely results in the unexpected decrease in MO-OOA and isoprene-OA decrease after injecting β-caryophyllene. It is possible that the larger Q/Q_{exp} in Chamber_Af and the decrease in MO-OOA and isoprene-OA are a result of the limitation of PMF analysis, that is, PMF assumes constant mass spectra of OA factors. After β-caryophyllene SOA formation in the chamber, in order to optimize the overall fitting residual, PMF solver increases the concentrations of LO-OOA and COA, the mass spectra of which are

more similar to β-caryophyllene SOA, and decreases the concentration of MO-OOA and isoprene-OA, the mass spectra of which are less similar to β-caryophyllene SOA.

We would like to clarify that our conclusions are not dependent on if PMF has perfectly accounted for the newly formed SOA, mainly because similar issues could also happen in the analysis of ambient data. The β-caryophyllene perturbation experiments simulate a scenario when there is a sudden change in the OA composition caused by an airmass encountering a plume or change in OA sources due to shift in wind direction. Under these circumstances, PMF analysis may have difficulty in accurately apportioning the OA sources. The simulated scenarios and the observed PMF issues have been observed in previous studies. For example, in the Figure 9 of Sun et al. (2016), an increase of hydrocarbon-like OA (HOA) is usually accompanied by a decrease in cooking OA (COA) and verse vice. Another example is that figure 5 of Reyes-Villegas et al. (2018) showed that a biomass burning plume leads to unexpected rapid variations in the concentration of many OA factors on the time scale of minutes. Last example is that in the figure S10 of Milic et al. (2017), the PMF residual during a biomass burning plume is orders of magnitude higher than other sampling periods.

S4. Description of Measurements at GT Site in Different Years

In addition to the perturbation experiments in 2016, we deployed AMS measurements in summer of 2012, 2013, and 2015 (Table S5) at the GT site (Xu et al., 2015a; Xu et al., 2017). The same five OA factors are resolved and the mass fractions of these OA factors do not change substantially over the past 5 years (Fig. S14), suggesting relatively stable OA sources over the past 5 years near this measurement site.

The 2012 measurements are used for the pseudo-experiment discussed in Appendix A. It is because the 2012 data set has the least interruption in ambient measurements. For example, in 2016, the perturbation experiments resulted in many gaps in the ambient measurements. In 2013, AMS alternated sampling between ambient line and a treated sampling line every 30min (Xu et al., 2017). Since measurements were performed around similar time of year each year and the mass fractions of these OA factors remain relatively constant over the past 5 years, this justifies the use 2012 data set for the pseudo-experiment (i.e., this data set can be considered as representative of other years).

S5. Community Multiscale Air Quality (CMAQ) Model

We use the CMAQ (Community Multiscale Air Quality) atmospheric chemical transport model to simulate the SOA formation in the southeastern U.S. CMAQ is one of the most widely used air quality models. CMAQ v5.2gamma (available at: https://github.com/USEPA/CMAQ) is run over the continental U.S. for time periods between May 2012 to July 2013 with 12km × 12km horizontal resolution. We focus our analysis on the southeastern U.S., which comprises 11 states (as Arkansas, Alabama, Florida, Georgia, Kentucky, Louisiana, Mississippi, North Carolina, South Carolina, Tennessee, and Virginia). 10 days of model spin-up are discarded before comparisons are made with measurements. The meteorological inputs are generated with version 3.8 of the Weather Research and Forecasting model (WRF), Advanced Research WRF (ARW) core. Compared to previous versions of WRF, WRF v3.8 has major revisions in the vertical mixing scheme (Appel et al., 2017). We also apply lightning assimilation to improve convective rainfall (Heath et al., 2016). Anthropogenic emissions are based on the EPA (Environmental Protection Agency) NEI (National Emission Inventory) 2011 v2. For the CTR_June period, the primary emissions from stationary source fuel combustion and industry are reduced to half in Alabama, because previous studies showed that CMAQ overestimates the primary organic carbon in Alabama during this period (Pye et al., 2015). Biogenic emissions are predicted by the BEIS (Biogenic Emission Inventory System) v3.6.1. Carlton and Baker (2011) found that the BEIS predicted isoprene emission is generally lower than that predicted by another widely used model MEGAN (Model of Emissions of Gases and Aerosols from Nature). Also, Pye et al. (2017) showed that increasing the BEIS predicted isoprene emission by 50% could result in a better agreement with measured isoprene and OH at Centreville, AL. Thus, the isoprene emission is increased by 50% in this study.

The gas-phase chemistry is based on CB6r3 (Carbon Bond v6.3, http://www.camx.com/files/udaq_snowchem_final_6aug15.pdf). The default organic aerosol treatment in CMAQ v5.2gamma generally follows the scheme of Carlton et al. (2010) and Appel et al. (2017) and is the same as that publicly released in CMAQ v5.2 and v5.2.1 (doi:10.5281/zenodo.1212601). A schematic of SOA treatment in CMAQ v5.2 is shown in Fig. S2a. In brief, CMAQ v5.2 includes SOA formation from anthropogenic and biogenic emissions. Anthropogenic precursors include benzene, toluene, xylene, long-chain alkanes (such as heptadecane), and PAHs (such as naphthalene). Biogenic precursors include isoprene,

monoterpenes, and sesquiterpenes. An Odum 2-product parameterization is used to describe SOA formation from these precursors. The SOA yields from monoterpene reactions with different oxidants (OH, ozone) are assumed to be the same and are based on daylight experiments of Griffin et al. (1999) The SOA yield from sesquiterpenes oxidation is parameterized in an analogous way as that of monoterpenes (Carlton et al., 2010). Five different species of monoterpenes are lumped into one species (i.e., TERP) according to U.S. emissions-based weighting factors. SOA formation from the reactive uptake of IEPOX and methacryloylperoxynitrate (MPAN) (isoprene oxidation products) onto aqueous aerosol is included. All semi-volatile OA in the model can undergo particle-phase oligomerization to produce non-volatile OA with a 29hr lifetime. POA is treated as semi-volatile. A parameterization to consider the SOA from semivolatile and intermediate volatility organic compounds (SVOC and IVOC, the emissions of which may not be characterized in current emission inventories) as well as other missing sources of SOA from anthropogenic combustion (potentially due to underestimated yields) is implemented (Murphy et al., 2017b).

The "default simulation" applies the default treatment of SOA in CMAQ v5.2 with CB6r3 as discussed above. The "updated simulation" in this work improves the "default simulation" by implementing the following recent scientific findings (Fig. S2b). Firstly, recent laboratory studies reveal significant amount of SOA formation from monoterpenes (except α-pinene, denoted as $MT_{w/o\ \alpha\text{-pinene}}$) oxidation by NO_3 (Boyd et al., 2015; Fry et al., 2014). This SOA formation pathway is currently missing in CMAQ v5.2 with CB6r3 chemistry. We implement the formation and partition of organic nitrates from monoterpenes via multiple reaction pathways (i.e., oxidation by NO_3 and oxidation by OH/O_3 followed by RO_2+NO), which are extensively described in Pye et al. (2015). In brief, the organic nitrates produced from $MT_{w/o\ \alpha\text{-pinene}}$ oxidation by NO_3 and MT oxidation by OH and O_3 in the presence of NO_x are lumped into a new species: $MTNO_3$. $MTNO_3$ is semi-volatile and undergoes gas/particle partitioning. The particle-phase $MTNO_3$ hydrolyzes with a 3hr lifetime and converts to HNO_3 and non-volatile SOA (denoted as AMTHYD in model). We note that the hydrolysis rate of organic nitrates is highly uncertain, which largely depends on the structure of organic nitrates and particle acidity (Boyd et al., 2015; Jacobs et al., 2014; Rindelaub et al., 2016). Pye et al. compared model performance using 3hr vs 30hr hydrolysis rate (Pye et al., 2015). While the 3hr hydrolysis rate leads to better agreements with measured OC and NO_y, it degrades the comparison with measured HNO_3. In this study, we perform sensitivity study by using both 3hr and 30hr hydrolysis rate. 30hr hydrolysis lower the modeled SOA_{MT+SQT}

concentration by 2-17% for all sites compared to 3hr hydrolysis, but it does not change the conclusion of this study. Future studies are warranted to constrain the fate of organic nitrates.

The second modification is to update the SOA yield of the monoterpenes oxidation by O_3 and OH. In the default SOA treatment, the SOA yield of lumped monoterpenes oxidation by O_3 and OH is parameterized based on daylight experiments of Griffin et al. (1999), which are under high OA loadings and elevated temperature. Extrapolation of the parameterized yield to atmospherically relevant low OA loading and lower temperatures (<310K) causes uncertainty (Pathak et al., 2007). In this study, we update the SOA yield of monoterpenes oxidation by O_3 and OH based on a recent study by Saha and Grieshop (2016). Saha et al. applied a dual-thermodenuder system to study the α-pinene ozonolysis SOA. The authors extracted SOA yield parameters by using an evaporation-kinetics model and volatility basis set (VBS). The SOA yields in Saha et al. (2016) are higher than laboratory chamber studies conducted in batch mode (Griffin et al., 1999; Pathak et al., 2007), but comparable to laboratory chamber studies conducted in continuous mode (Shilling et al., 2008) (Fig. S15). The SOA yields in Saha et al. are consistent with recent findings about the formation of HOMs (Ehn et al., 2014; Zhang et al., 2015) and help to explain the observed slow evaporation of α-pinene SOA (Vaden et al., 2011). In the updated simulation, we replace the Odum's 2-product model used in the default simulation with VBS framework. The VBS framework lumps species into a number of volatility "bins" that are separated by one decade in saturation concentration. When laboratory data are available over a wide range of loadings and/or temperatures, the VBS framework is more robust and better represents SOA formation at atmospherically relevant OA loadings than Odum's 2-product model with limited data (Barsanti et al., 2013). In addition, the new parameterization allows for enthalpies of vaporization that are more consistent with species of the specified volatility. Specifically, CMAQ has used enthalpies of vaporization of 40 kJ mol^{-1} for C* of 15 and 134 μg m^{-3}. Species of this saturation concentration should have much enthalpies of vaporization on the order of 100 kJ mol^{-1} (Epstein et al., 2010). The new parameterization from Saha et al. allows for higher enthalpies of vaporization that are more realistic. The properties of the lumped MT oxidation products, which are grouped into 7 volatility "bins", are listed in Table S3. The simulation using modified SOA treatment is denoted as "updated simulation".

The modeled OA concentrations from both default simulation and updated simulation are compared to AMS measurements. Considering that CMAQ predicts aerosol in 3 log-normal modes

and AMS measures PM_1, the modeled mass concentration is adjusted to PM_1 based on predicted aerosol size distributions (Nolte et al., 2015). CMAQ predicts that PM_1 concentration accounts for about 60-70% of $PM_{2.5}$ concentration. This fraction is similar to the finding in Zhang et al. (2017), who performed simultaneous measurements of non-refractory $PM_{2.5}$ (using an AMS with a new $PM_{2.5}$ inlet) and non-refractory PM_1 (using an AMS with a traditional PM_1 inlet) in Nanjing, China. The authors showed that non-refractory PM_1 accounts for about half of non-refractory $PM_{2.5}$. The $PM_1/PM_{2.5}$ fraction needs to be further verified for sites in the U.S.

Fig. S16 compares the diurnal trends of AMS OA with CMAQ OA in both default simulation and updated simulation. The JST and GT sites are in the same grid cell in CMAQ. The modeled OA in default simulation under-estimates measured OA by 36-54%. The updated simulation predicts more OA, which reduces model bias and agrees better with measured OA. The model skill in updated simulation is slightly improved as the correlation between model and measurement is better (Fig. S17). However, the updated simulation still under-estimates OA, mainly in the afternoon, suggesting missing OA sources.

We further evaluate the modeled SOA from the oxidation of monoterpenes and sesquiterpenes (SOA_{MT+SQT}) against LO-OOA. Based on the ambient perturbation experiments, 84% of fresh α-pinene SOA is apportioned into LO-OOA and the rest 16% is apportioned into isoprene-OA (Fig. S5a), when the isoprene-OA factor exists. Thus, for the sites with isoprene-OA factor, we only consider 84% of modeled SOA from the oxidation of monoterpenes by O_3 and OH when comparing to LO-OOA. We note that the fraction of MT SOA apportioned into isoprene-OA factor is uncertain, as this value is obtained at a specific site and in a specific month. This uncertainty may affect the comparison between modeled SOA_{MT+SQT} and LO-OOA. More studies are required to evaluate the interference of MT SOA in isoprene-OA factor in different atmospheric environments and different seasons. The comparison between LO-OOA and SOA_{MT+SQT} is discussed in the main text and shown in Fig. S18, Fig. S19, Fig. S20, and Fig. 6. The SOA_{MT+SQT} concentration in the default simulation (i.e., no explicit organic nitrate partitioning, Griffin et al. (1999) photooxidation parameterization) is significantly lower than LO-OOA by 55-84% (Fig. S20). In contrast, SOA_{MT+SQT} in the updated simulation (explicit organic nitrates and Saha and Grieshop (2016) VBS for $MT+O_3/OH$) reasonably reproduces the magnitude and diurnal variability of LO-OOA for each site (Fig. 6a). The model bias is reduced to within ~20% for most sites, except for Centreville, Alabama (i.e., 43% for CTR_June dataset). For CTR_June, the

modeled SOA_{MT+SQT} is higher than LO-OOA by ~43%. The reason for the over-estimation of LO-OOA in CTR_June is unclear. One possible reason is that CMAQ over-predicts the role of primary organic emissions and subsequent OA formation from these emissions, which serve as gas/particle partition medium. This suggests that the parameterized potential SOA from combustion sources (i.e., pcSOA) may need downward adjustment (Murphy et al., 2017b). The sampling site in CTR is surrounded by forests and is far away from stationary point and area sources of primary emissions. The marginal influence of primary emissions on the CTR site can be reflected by that HOA factor is not resolved from PMF analysis. However, the grid cell containing the CTR site has primary emissions. Pye et al. (2015) showed that the POA concentration is over-estimated by a factor of 2 in CTR_June when POA is treated as non-volatile. As gas/particle partition medium, a higher POA concentration would enhance the partition of semi-volatiles to the particle phase and hence increase the concentration of modeled SOA. The implementation of SOA formation from SVOC and IVOC, mainly from anthropogenic emissions, further exaggerates the issue. Another possible reason is that the parameterization of MT SOA formation does not consider photo-chemical aging. The laboratory experiments used to derive SOA yield parameters typically only last few hours. The aging of SOA is likely to decrease the concentration after long time periods due to fragmentation. In addition, previous work by Pye et al. (2015), albeit with different meteorology indicates monoterpenes as well as their organic nitrates are overestimated by CMAQ in the vicinity of CTR. Errors in nocturnal mixing may contribute to errors in SOA, particularly from monoterpenes.

S6. Simple Box Model

While the focus of this study is to qualitatively understand which OA factors the α-pinene SOA is apportioned into, we also build a simple box model aimed at quantitatively estimating the fate of α-pinene and the SOA formation in the ambient perturbation experiments. The box model considers the oxidation of α-pinene by OH and O_3, dilution by ambient air, and particle loss to chamber wall. We solve the following two ordinary differential equations (ODEs) which are derived from mass balance.

$$\frac{d[\alpha\text{-pinene}]}{dt} = -k_{OH}\times[\alpha\text{-pinene}]\times[OH] - k_{O_3}\times[\alpha\text{-pinene}]\times[O_3] - \frac{F_{out}}{V_{chamber}}\times[\alpha\text{-pinene}] \quad \text{Eq. S1}$$

$$\frac{d[SOA]}{dt} = Yield \times (k_{OH}\times[\alpha\text{-pinene}]\times[OH] + k_{O_3}\times[\alpha\text{-pinene}]\times[O_3])\times 5.6 - \frac{F_{out}}{V_{chamber}}\times[SOA] - k_{wall\text{-}loss}\times[SOA] \quad \text{Eq. S2}$$

F_{out} is the dilution rate, which is 20 LPM (estimated by sampling flow rates of all instruments). $V_{chamber}$ is the chamber volume, which is about 2 m^3. k_{OH} and k_{O3} are the reaction rate constants for α-pinene + OH and α-pinene + O_3,which are 5.25×10^{-11} and 9.40×10^{-17} cm^3 $molecule^{-1}$ s^{-1} at 298K, respectively (Jenkin et al., 1997). The constant 5.6 is to convert the α-pinene concentration unit from ppb to μg m^{-3}. *Yield* is defined as the ratio of the amount of SOA formed to the amount of VOC reacted (Odum et al., 1996), which is assumed to the same for the oxidation of α-pinene by OH and O_3. The ambient perturbation approach is potentially feasible to directly measure the SOA yield under real atmospheric conditions. However, certain improvements are required, such as measuring the concentration of precursor VOC and quantifying the dilution ratio. In the current box model, *yield* is a tuning parameter. The model only considers the SOA formed from α-pinene injected into the chamber and neglects the inflow ambient OA and α-pinene. Thus, the model results can be directly compared to the LO-OOA enhancement amount.

We use the simple box model to simulate experiment ap_0801_1. The O_3 concentration measured during this experiment is ~55 ppb. The OH concentration is not measured, but assumed to be 1×10^6 or 2×10^6 molecule cm^{-3} as sensitivity tests. The particle wall loss is difficult to characterize because the eight corners of the bag are open, so that the change in particle number concentration can be due to both wall loss and ambient variation. Moreover, the particle wall loss may vary between experiments because the wind affects the movement of chamber walls and hence the particle wall loss. Thus, we assume the particle wall loss rate to be 1×10^{-4} s^{-1}, which is 100 times higher than the loss rate of 200nm particles in the Georgia Tech Environmental Chamber facility (Nah et al., 2016) and serves as an upper bound of loss rate. We find that the wall loss rate has negligible effects on particle mass concentration, compared to other factors.

Fig. S21 shows the results from the simple box model. Although ~14 ppb α-pinene is injected, most of α-pinene is carried out of the chamber due to dilution with ambient air (Fig. S21a). Only 2-5 ppb α-pinene reacts with oxidants (i.e., O_3 and OH) after 40 min. For the reacted α-pinene, roughly half reacts with O_3 and the other half reacts with OH. Fig. S21a also shows the simulated time series of SOA by using a range of yields. The box model can predict the measured enhancement amount in SOA using SOA yields of 20-30%, which is consistent with yields measured from laboratory studies (Saha and Grieshop, 2016; Shilling et al., 2008). Despite the agreement in magnitude, the predicted SOA concentration peaks later and decreases slower than measurements. Possible reasons include non-ideal mixing and/or existence of a dead zone in the

chamber. Assuming a 1.75 m^3 dead zone in the 2 m^3 chamber can reasonably simulate the temporal profile of measured SOA (Fig. S21b) with a 10-15 % SOA yield. Roughly 10ppb α-pinene (10% of initial concentration) is consumed by O_3. This amount likely serves as an upper bound because a 10ppb decrease in O_3 concentration is not observed any experiments. Another uncertain parameter in the box model is the dilution rate. Increasing the dilution rate would have the same effect as increasing the volume of dead zone. The dilution rate is estimated to be 20 LPM as determined by the pulling rates of all instruments. This dilution rate is better constrained than the volume of dead zone since the instrument sampling rates are known. The reasons for the discrepancy in OA decrease rate between model and measurements are unclear, but likely due to a combination of dead zone volume and dilution rate. To understand this discrepancy, future studies with adequate measurements of more species, particularly the VOCs, are required. The improved experiments could provide better estimate of SOA yields under real ambient conditions. Palm et al. (2017) attempted to quantify the SOA yields from the individual VOC by oxidizing VOC in an oxidation flow reactor (OFR) with ambient air. Note that the extra oxidation is added in the OFR in Palm et al. (2017), which is different from this study. The discrepancy between model and measurements in either the magnitude or the decrease rate does not influence the conclusions in this study, as our focus is to qualitatively understand which OA factors the α-pinene SOA is apportioned into.

The OA formation in perturbation experiments with isoprene or *m*-xylene is below the detection limit of the experimental approach. This is mainly due to the low SOA yields or slow oxidation rates of these VOCs (Ng et al., 2007). We used the simple box model to simulate the perturbation experiments with isoprene and *m*-xylene. For *m*-xylene experiments, about 90 ppb is injected. However, due to the slow oxidation rate of *m*-xylene, small SOA yield (i.e., ~5% in Ng et al. (2007)), and large dilution by ambient air, it is estimated that only about 4 ppb *m*-xylene reacts with OH after 40min and produces ~0.15-0.30 μg m^{-3} SOA (Fig. S21c). For isoprene, although its oxidation rate is fast, its SOA yield from non-IEPOX route is low (Xu et al., 2014; Kroll et al., 2006). The isoprene oxidation products which form SOA are mostly second or higher generation products. They are not formed in large amount in the relatively short perturbation experiments (i.e., 40min). The lack of SOA formation in naphthalene experiments is probably due to naphthalene was not adequately injected into chamber. We injected naphthalene by passing pure air (1 liter per min) over the solid naphthalene under ambient temperature for 1 min. Due to the

relatively low vapor pressure of naphthalene (23.6Pa at 30°C) and rapid dilution in the chamber, the injected naphthalene concentration could be very low.

S7. Laboratory Study on SOA Formation from α-pinene

We performed laboratory experiments to study the SOA formation from α-pinene under different NO_x conditions in the Georgia Tech Environmental Chamber (GTEC) facility. The facility consists of two 12 m^3 Teflon chambers, which are suspended inside a temperature-controlled enclosure and surrounded by black lights. The detailed description about chamber facility can be found in Boyd et al. (2015) The experimental procedures have been discussed in Tuet et al. (2017) In brief, the chambers are flushed with clean air prior to each experiment. Then, α-pinene and oxidant sources (i.e., H_2O_2, NO_2, or HONO) are injected into chamber. Once the concentrations of species stabilize, the black lights are turned on to initiate photooxidation. The SOA generated by using H_2O_2 (i.e., NO-free condition), NO_2 (i.e., mid-NO condition), and HONO (i.e., high NO condition) as oxidant sources are denoted as $SOA_{lab,H2O2}$, $SOA_{lab,NO2}$, and $SOA_{lab,HONO}$, respectively.

The experimental conditions are summarized in Table S2. We note that more than 100ppb α-pinene is injected in the experiments using H_2O_2 and HONO. It is because these two experiments were designed to produce large amounts of SOA for filter collection and offline analysis (Tuet et al., 2017). Considering that the OA concentration affects the partitioning of semi-volatile organic compounds and hence affects the organic mass spectra measured by AMS, we calculate the average mass spectra in these laboratory studies by only using the data when the OA concentration is below 10 μg m^{-3}, which is similar to that in our ambient perturbation experiments.

The mass spectra of each laboratory-generated SOA (denoted as SOA_{lab}) are compared against the mass spectra of α-pinene SOA generated during perturbation experiments (denoted as "$SOA_{ambient}$"). The correlation coefficients (R) between the mass spectra of SOA_{lab} and $SOA_{ambient}$ are plotted against the NO concentration during ambient perturbation experiments. We calculate the organic mass spectra of $SOA_{ambient}$ in the following way. Firstly, we scale the magnitude of the OA mass spectrum during Chamber_Bf period by the ratio of OA concentration during the Chamber_Bf period to that during the extrapolated Chamber_Bf period. Secondly, we subtract this scaled OA mass spectrum from that during the Chamber_Af period. Thirdly, we normalize the "difference mass spectra" to the difference in organic signal. It is important to note that this

463 calculation is only performed for the experiments with significant formation of total OA. The
464 comparison results are discussed in the main text.

465 When comparing the mass spectra of $SOA_{ambient}$ with SOA_{lab}, we note that the mass
466 spectrua of $SOA_{ambient}$ (when ambient NO is > 0.3ppb) generally agree better with that of
467 $SOA_{lab,NO2}$ than $SOA_{lab,HONO}$. This suggest that the laboratory experiment using NO_2+hν as oxidant
468 source is more representative of ambient high NO conditions than HONO+hν. This is likely due
469 to the following reasons. Firstly, from the simple box model, we estimate that about half of α-
470 pinene reacts with OH and the other half reacts with O_3 in the perturbation experiments, which is
471 similar to that in laboratory experiments with NO_2+hν (Table S2). In contrast, the fate of α-pinene
472 is dominated by OH in HONO+hν experiment. Secondly, the NO_x level and NO/NO_2 ratio in
473 perturbation experiments are more similar to those in the NO_2+hν experiment than the HONO
474 experiment. For example, the NO/NO_2 ratio in α-pinene perturbation experiments ranges between
475 0.03 and 0.4, which is closer to the range in NO_2+hν experiment (0.1-0.4) than in HONO
476 experiment (0.4-0.9). Thirdly, while both perturbation experiments and NO_2+hν experiment have
477 high RH (>40%), the RH in HONO+hν experiment is <5%. However, we expect the effects of
478 different RH on the mass spectra comparison are much smaller compared to the first two reasons.

479 **S8. Estimate the Fate of RO_2 in the Atmosphere**

480 The plateaus in Fig. 7 indicate that when NO is ~0.3ppb, RO_2+NO is the dominant fate of
481 RO_2. This NO level (~0.3ppb) is consistent with the NO level required to dominate the fate of RO_2,
482 as calculated by using previously measured HO_2 and kinetic rate constants.

483 According to Master Chemical Mechanism (MCM v3.3) (Jenkin et al., 1997; Saunders et
484 al., 2003), the reaction rates of RO_2+NO and RO_2+HO_2 are listed below.

485
$$k_{RO_2+NO} = 2.7e\text{-}12\times\exp(360/T) = 9.04e\text{-}12\ cm^3\ molecule^{-1}\ s^{-1}\ (@298K)$$
$$k_{RO_2+HO_2} = 2.91e\text{-}13\times\exp(1300/T) = 2.28e\text{-}11\ cm^3\ molecule^{-1}\ s^{-1}\ (@298K)$$

486 The afternoon HO_2 concentration is about 5-20ppt from previous measurements at the same site
487 during a similar period (Sanchez et al., 2016; Chen et al., 2017). Thus, when the NO concentration
488 is about 0.1-0.5 ppb, RO_2+NO would be 10 times faster than RO_2+HO_2 and NO dominates the fate
489 of RO_2. This is similar to the estimated 0.2-0.3 ppb based on the comparison in organic mass
490 spectra between $SOA_{ambient}$ and SOA_{lab}.

S9. More discussions on β-caryophyllene perturbation experiments.

One interesting finding in β-caryophyllene perturbation experiments is that the LO-OOA enhancement amount is greatly affected by NO_2 level. More LO-OOA is formed in perturbation experiments with a lower NO_2 level (Fig. S22f), when the O_3 concentration and injection time are similar. The reason for this NO_2 effect on β-caryophyllene SOA is currently unknown. Considering that the major fate of β-caryophyllene in the ambient perturbation experiments is reaction with O_3 (i.e., lifetimes of β-caryophyllene with respect to 40ppb O_3 and 10^6 molecules cm^{-3} OH are 1.5min and 80min, respectively), the NO_2 effect may be related to Criegee radical, which is the most important intermediate radical in ozonolysis of alkenes. In terms of the roles of NO_x in SOA formation from β-caryophyllene, previous laboratory studies have mostly focused on the β-caryophyllene oxidation by OH (Tasoglou and Pandis, 2015) instead of oxidation by O_3 (i.e., the atmospherically dominant fate of β-caryophyllene). Thus, the effects of NO_2 on SOA formation from the ozonolysis of β-caryophyllene warrants future studies.

Reference

Appel, K. W., Napelenok, S. L., Foley, K. M., Pye, H. O. T., Hogrefe, C., Luecken, D. J., Bash, J. O., Roselle, S. J., Pleim, J. E., Foroutan, H., Hutzell, W. T., Pouliot, G. A., Sarwar, G., Fahey, K. M., Gantt, B., Gilliam, R. C., Heath, N. K., Kang, D., Mathur, R., Schwede, D. B., Spero, T. L., Wong, D. C., and Young, J. O.: Description and evaluation of the Community Multiscale Air Quality (CMAQ) modeling system version 5.1, Geosci. Model Dev., 10, 1703-1732, 10.5194/gmd-10-1703-2017, 2017.

Bahreini, R., Keywood, M. D., Ng, N. L., Varutbangkul, V., Gao, S., Flagan, R. C., Seinfeld, J. H., Worsnop, D. R., and Jimenez, J. L.: Measurements of Secondary Organic Aerosol from Oxidation of Cycloalkenes, Terpenes, and m-Xylene Using an Aerodyne Aerosol Mass Spectrometer, Environ Sci Technol, 39, 5674-5688, 10.1021/es048061a, 2005.

Barsanti, K. C., Carlton, A. G., and Chung, S. H.: Analyzing experimental data and model parameters: implications for predictions of SOA using chemical transport models, Atmos. Chem. Phys., 13, 12073-12088, 10.5194/acp-13-12073-2013, 2013.

Bougiatioti, A., Stavroulas, I., Kostenidou, E., Zarmpas, P., Theodosi, C., Kouvarakis, G., Canonaco, F., Prévôt, A. S. H., Nenes, A., Pandis, S. N., and Mihalopoulos, N.: Processing of biomass-burning aerosol in the eastern Mediterranean during summertime, Atmos. Chem. Phys., 14, 4793-4807, 10.5194/acp-14-4793-2014, 2014.

Boyd, C. M., Sanchez, J., Xu, L., Eugene, A. J., Nah, T., Tuet, W. Y., Guzman, M. I., and Ng, N. L.: Secondary organic aerosol formation from the β-pinene+NO3 system: effect of humidity and peroxy radical fate, Atmos. Chem. Phys., 15, 7497-7522, 10.5194/acp-15-7497-2015, 2015.

Budisulistiorini, S. H., Canagaratna, M. R., Croteau, P. L., Marth, W. J., Baumann, K., Edgerton, E. S., Shaw, S. L., Knipping, E. M., Worsnop, D. R., Jayne, J. T., Gold, A., and Surratt, J. D.: Real-Time Continuous Characterization of Secondary Organic Aerosol Derived from Isoprene Epoxydiols in Downtown Atlanta, Georgia, Using the Aerodyne Aerosol Chemical Speciation Monitor, Environ Sci Technol, 47, 5686-5694, Doi 10.1021/Es400023n, 2013.

Budisulistiorini, S. H., Li, X., Bairai, S. T., Renfro, J., Liu, Y., Liu, Y. J., McKinney, K. A., Martin, S. T., McNeill, V. F., Pye, H. O. T., Nenes, A., Neff, M. E., Stone, E. A., Mueller, S., Knote, C., Shaw, S. L., Zhang, Z., Gold, A., and Surratt, J. D.: Examining the effects of anthropogenic emissions on isoprene-derived secondary organic aerosol formation during the 2013 Southern Oxidant and Aerosol Study (SOAS) at the Look Rock, Tennessee ground site, Atmos. Chem. Phys., 15, 8871-8888, 10.5194/acp-15-8871-2015, 2015.

Canagaratna, M. R., Jayne, J. T., Jimenez, J. L., Allan, J. D., Alfarra, M. R., Zhang, Q., Onasch, T. B., Drewnick, F., Coe, H., Middlebrook, A., Delia, A., Williams, L. R., Trimborn, A. M.,

548 Northway, M. J., DeCarlo, P. F., Kolb, C. E., Davidovits, P., and Worsnop, D. R.: Chemical and
549 microphysical characterization of ambient aerosols with the aerodyne aerosol mass spectrometer,
550 Mass Spectrometry Reviews, 26, 185-222, 10.1002/mas.20115, 2007.
551
552 Canagaratna, M. R., Jimenez, J. L., Kroll, J. H., Chen, Q., Kessler, S. H., Massoli, P., Hildebrandt
553 Ruiz, L., Fortner, E., Williams, L. R., Wilson, K. R., Surratt, J. D., Donahue, N. M., Jayne, J. T.,
554 and Worsnop, D. R.: Elemental ratio measurements of organic compounds using aerosol mass
555 spectrometry: characterization, improved calibration, and implications, Atmos. Chem. Phys., 15,
556 253-272, 10.5194/acp-15-253-2015, 2015.
557
558 Carlton, A. G., Bhave, P. V., Napelenok, S. L., Edney, E. O., Sarwar, G., Pinder, R. W., Pouliot,
559 G. A., and Houyoux, M.: Model Representation of Secondary Organic Aerosol in CMAQv4.7,
560 Environ Sci Technol, 44, 8553-8560, 10.1021/es100636q, 2010.
561
562 Carlton, A. G., and Baker, K. R.: Photochemical Modeling of the Ozark Isoprene Volcano:
563 MEGAN, BEIS, and Their Impacts on Air Quality Predictions, Environ Sci Technol, 45, 4438-
564 4445, 10.1021/es200050x, 2011.
565
566 Chan, M. N., Chan, A. W. H., Chhabra, P. S., Surratt, J. D., and Seinfeld, J. H.: Modeling of
567 secondary organic aerosol yields from laboratory chamber data, Atmos. Chem. Phys., 9, 5669-
568 5680, 10.5194/acp-9-5669-2009, 2009.
569
570 Chen, D., Huey, L. G., Tanner, D. J., Li, J., Ng, N. L., and Wang, Y.: Derivation of Hydroperoxyl
571 Radical Levels at an Urban Site via Measurement of Pernitric Acid by Iodide Chemical Ionization
572 Mass Spectrometry, Environ Sci Technol, 10.1021/acs.est.6b05169, 2017.
573
574 Chen, Q., Farmer, D. K., Rizzo, L. V., Pauliquevis, T., Kuwata, M., Karl, T. G., Guenther, A.,
575 Allan, J. D., Coe, H., Andreae, M. O., Pöschl, U., Jimenez, J. L., Artaxo, P., and Martin, S. T.:
576 Submicron particle mass concentrations and sources in the Amazonian wet season (AMAZE-08),
577 Atmos. Chem. Phys., 15, 3687-3701, 10.5194/acp-15-3687-2015, 2015.
578
579 Crippa, M., Canonaco, F., Lanz, V. A., Äijälä, M., Allan, J. D., Carbone, S., Capes, G., Ceburnis,
580 D., Dall'Osto, M., Day, D. A., DeCarlo, P. F., Ehn, M., Eriksson, A., Freney, E., Hildebrandt Ruiz,
581 L., Hillamo, R., Jimenez, J. L., Junninen, H., Kiendler-Scharr, A., Kortelainen, A. M., Kulmala,
582 M., Laaksonen, A., Mensah, A. A., Mohr, C., Nemitz, E., O'Dowd, C., Ovadnevaite, J., Pandis, S.
583 N., Petäjä, T., Poulain, L., Saarikoski, S., Sellegri, K., Swietlicki, E., Tiitta, P., Worsnop, D. R.,
584 Baltensperger, U., and Prévôt, A. S. H.: Organic aerosol components derived from 25 AMS data
585 sets across Europe using a consistent ME-2 based source apportionment approach, Atmos. Chem.
586 Phys., 14, 6159-6176, 10.5194/acp-14-6159-2014, 2014.
587
588 de Sá, S. S., Palm, B. B., Campuzano-Jost, P., Day, D. A., Newburn, M. K., Hu, W., Isaacman-
589 VanWertz, G., Yee, L. D., Thalman, R., Brito, J., Carbone, S., Artaxo, P., Goldstein, A. H., Manzi,
590 A. O., Souza, R. A. F., Mei, F., Shilling, J. E., Springston, S. R., Wang, J., Surratt, J. D., Alexander,

591 M. L., Jimenez, J. L., and Martin, S. T.: Influence of urban pollution on the production of organic
592 particulate matter from isoprene epoxydiols in central Amazonia, Atmos. Chem. Phys. Discuss.,
593 2016, 1-58, 10.5194/acp-2016-1020, 2016.
594
595 de Sá, S. S., Palm, B. B., Campuzano-Jost, P., Day, D. A., Newburn, M. K., Hu, W., Isaacman-
596 VanWertz, G., Yee, L. D., Thalman, R., Brito, J., Carbone, S., Artaxo, P., Goldstein, A. H., Manzi,
597 A. O., Souza, R. A. F., Mei, F., Shilling, J. E., Springston, S. R., Wang, J., Surratt, J. D., Alexander,
598 M. L., Jimenez, J. L., and Martin, S. T.: Influence of urban pollution on the production of organic
599 particulate matter from isoprene epoxydiols in central Amazonia, Atmos. Chem. Phys., 17, 6611-
600 6629, 10.5194/acp-17-6611-2017, 2017.
601
602 DeCarlo, P. F., Kimmel, J. R., Trimborn, A., Northway, M. J., Jayne, J. T., Aiken, A. C., Gonin,
603 M., Fuhrer, K., Horvath, T., Docherty, K. S., Worsnop, D. R., and Jimenez, J. L.: Field-Deployable,
604 High-Resolution, Time-of-Flight Aerosol Mass Spectrometer, Anal Chem, 78, 8281-8289,
605 10.1021/ac061249n, 2006.
606
607 Donahue, N. M., Epstein, S. A., Pandis, S. N., and Robinson, A. L.: A two-dimensional volatility
608 basis set: 1. organic-aerosol mixing thermodynamics, Atmos. Chem. Phys., 11, 3303-3318,
609 10.5194/acp-11-3303-2011, 2011.
610
611 Ehn, M., Thornton, J. A., Kleist, E., Sipila, M., Junninen, H., Pullinen, I., Springer, M., Rubach,
612 F., Tillmann, R., Lee, B., Lopez-Hilfiker, F., Andres, S., Acir, I.-H., Rissanen, M., Jokinen, T.,
613 Schobesberger, S., Kangasluoma, J., Kontkanen, J., Nieminen, T., Kurten, T., Nielsen, L. B.,
614 Jorgensen, S., Kjaergaard, H. G., Canagaratna, M., Maso, M. D., Berndt, T., Petaja, T., Wahner,
615 A., Kerminen, V.-M., Kulmala, M., Worsnop, D. R., Wildt, J., and Mentel, T. F.: A large source
616 of low-volatility secondary organic aerosol, Nature, 506, 476-479, 10.1038/nature13032, 2014.
617
618 Epstein, S. A., Riipinen, I., and Donahue, N. M.: A Semiempirical Correlation between Enthalpy
619 of Vaporization and Saturation Concentration for Organic Aerosol, Environ Sci Technol, 44, 743-
620 748, Doi 10.1021/Es902497z, 2010.
621
622 Fry, J. L., Draper, D. C., Barsanti, K. C., Smith, J. N., Ortega, J., Winkler, P. M., Lawler, M. J.,
623 Brown, S. S., Edwards, P. M., Cohen, R. C., and Lee, L.: Secondary Organic Aerosol Formation
624 and Organic Nitrate Yield from NO3 Oxidation of Biogenic Hydrocarbons, Environ Sci Technol,
625 48, 11944-11953, 10.1021/es502204x, 2014.
626
627 Griffin, R. J., Cocker, D. R., Flagan, R. C., and Seinfeld, J. H.: Organic aerosol formation from
628 the oxidation of biogenic hydrocarbons, J Geophys Res-Atmos, 104, 3555-3567, Doi
629 10.1029/1998jd100049, 1999.
630
631 Guenther, A., Jiang, X., Heald, C. L., Sakulyanontvittaya, T., Duhl, T., Emmons, L. K., and Wang,
632 X.: The Model of Emissions of Gases and Aerosols from Nature version 2.1 (MEGAN2.1): an

633 extended and updated framework for modeling biogenic emissions, Geosci. Model Dev., 5, 1471-
634 1492, 10.5194/gmd-5-1471-2012, 2012.
635
636 Heath, N. K., Pleim, J. E., Gilliam, R. C., and Kang, D.: A simple lightning assimilation technique
637 for improving retrospective WRF simulations, Journal of Advances in Modeling Earth Systems, 8,
638 1806-1824, 10.1002/2016MS000735, 2016.
639
640 Helmig, D., Ortega, J., Duhl, T., Tanner, D., Guenther, A., Harley, P., Wiedinmyer, C., Milford,
641 J., and Sakulyanontvittaya, T.: Sesquiterpene Emissions from Pine Trees − Identifications,
642 Emission Rates and Flux Estimates for the Contiguous United States, Environ Sci Technol, 41,
643 1545-1553, 10.1021/es0618907, 2007.
644
645 Hodzic, A., Aumont, B., Knote, C., Lee-Taylor, J., Madronich, S., and Tyndall, G.: Volatility
646 dependence of Henry's law constants of condensable organics: Application to estimate
647 depositional loss of secondary organic aerosols, Geophysical Research Letters, 41, 4795-4804,
648 10.1002/2014GL060649, 2014.
649
650 Hu, W. W., Campuzano-Jost, P., Palm, B. B., Day, D. A., Ortega, A. M., Hayes, P. L., Krechmer,
651 J. E., Chen, Q., Kuwata, M., Liu, Y. J., de Sá, S. S., McKinney, K., Martin, S. T., Hu, M.,
652 Budisulistiorini, S. H., Riva, M., Surratt, J. D., St. Clair, J. M., Isaacman-Van Wertz, G., Yee, L.
653 D., Goldstein, A. H., Carbone, S., Brito, J., Artaxo, P., de Gouw, J. A., Koss, A., Wisthaler, A.,
654 Mikoviny, T., Karl, T., Kaser, L., Jud, W., Hansel, A., Docherty, K. S., Alexander, M. L., Robinson,
655 N. H., Coe, H., Allan, J. D., Canagaratna, M. R., Paulot, F., and Jimenez, J. L.: Characterization
656 of a real-time tracer for isoprene epoxydiols-derived secondary organic aerosol (IEPOX-SOA)
657 from aerosol mass spectrometer measurements, Atmos. Chem. Phys., 15, 11807-11833,
658 10.5194/acp-15-11807-2015, 2015.
659
660 Huang, X. F., He, L. Y., Hu, M., Canagaratna, M. R., Sun, Y., Zhang, Q., Zhu, T., Xue, L., Zeng,
661 L. W., Liu, X. G., Zhang, Y. H., Jayne, J. T., Ng, N. L., and Worsnop, D. R.: Highly time-resolved
662 chemical characterization of atmospheric submicron particles during 2008 Beijing Olympic
663 Games using an Aerodyne High-Resolution Aerosol Mass Spectrometer, Atmos Chem Phys, 10,
664 8933-8945, DOI 10.5194/acp-10-8933-2010, 2010.
665
666 Jacobs, M. I., Burke, W. J., and Elrod, M. J.: Kinetics of the reactions of isoprene-derived
667 hydroxynitrates: gas phase epoxide formation and solution phase hydrolysis, Atmos. Chem. Phys.,
668 14, 8933-8946, 10.5194/acp-14-8933-2014, 2014.
669
670 Jenkin, M. E., Saunders, S. M., and Pilling, M. J.: The tropospheric degradation of volatile organic
671 compounds: a protocol for mechanism development, Atmospheric Environment, 31, 81-104,
672 http://dx.doi.org/10.1016/S1352-2310(96)00105-7, 1997.
673
674 Jimenez, J. L., Canagaratna, M. R., Donahue, N. M., Prevot, A. S. H., Zhang, Q., Kroll, J. H.,
675 DeCarlo, P. F., Allan, J. D., Coe, H., Ng, N. L., Aiken, A. C., Docherty, K. S., Ulbrich, I. M.,

676 Grieshop, A. P., Robinson, A. L., Duplissy, J., Smith, J. D., Wilson, K. R., Lanz, V. A., Hueglin,
677 C., Sun, Y. L., Tian, J., Laaksonen, A., Raatikainen, T., Rautiainen, J., Vaattovaara, P., Ehn, M.,
678 Kulmala, M., Tomlinson, J. M., Collins, D. R., Cubison, M. J., Dunlea, E. J., Huffman, J. A.,
679 Onasch, T. B., Alfarra, M. R., Williams, P. I., Bower, K., Kondo, Y., Schneider, J., Drewnick, F.,
680 Borrmann, S., Weimer, S., Demerjian, K., Salcedo, D., Cottrell, L., Griffin, R., Takami, A.,
681 Miyoshi, T., Hatakeyama, S., Shimono, A., Sun, J. Y., Zhang, Y. M., Dzepina, K., Kimmel, J. R.,
682 Sueper, D., Jayne, J. T., Herndon, S. C., Trimborn, A. M., Williams, L. R., Wood, E. C.,
683 Middlebrook, A. M., Kolb, C. E., Baltensperger, U., and Worsnop, D. R.: Evolution of Organic
684 Aerosols in the Atmosphere, Science, 326, 1525-1529, DOI 10.1126/science.1180353, 2009.
685

686 Keywood, M. D., Varutbangkul, V., Bahreini, R., Flagan, R. C., and Seinfeld, J. H.: Secondary
687 organic aerosol formation from the ozonolysis of cycloalkenes and related compounds, Environ
688 Sci Technol, 38, 4157-4164, Doi 10.1021/Es.035363o, 2004.
689

690 Kroll, J. H., Ng, N. L., Murphy, S. M., Flagan, R. C., and Seinfeld, J. H.: Secondary organic aerosol
691 formation from isoprene photooxidation, Environ Sci Technol, 40, 1869-1877, Doi
692 10.1021/Es0524301, 2006.
693

694 Lin, Y. H., Zhang, Z. F., Docherty, K. S., Zhang, H. F., Budisulistiorini, S. H., Rubitschun, C. L.,
695 Shaw, S. L., Knipping, E. M., Edgerton, E. S., Kleindienst, T. E., Gold, A., and Surratt, J. D.:
696 Isoprene Epoxydiols as Precursors to Secondary Organic Aerosol Formation: Acid-Catalyzed
697 Reactive Uptake Studies with Authentic Compounds, Environ Sci Technol, 46, 250-258, Doi
698 10.1021/Es202554c, 2012.
699

700 Liu, S., Aiken, A. C., Gorkowski, K., Dubey, M. K., Cappa, C. D., Williams, L. R., Herndon, S.
701 C., Massoli, P., Fortner, E. C., Chhabra, P. S., Brooks, W. A., Onasch, T. B., Jayne, J. T., Worsnop,
702 D. R., China, S., Sharma, N., Mazzoleni, C., Xu, L., Ng, N. L., Liu, D., Allan, J. D., Lee, J. D.,
703 Fleming, Z. L., Mohr, C., Zotter, P., Szidat, S., and Prevot, A. S. H.: Enhanced light absorption by
704 mixed source black and brown carbon particles in UK winter, Nat Commun, 6,
705 10.1038/ncomms9435, 2015.
706

707 Matthew, B. M., Middlebrook, A. M., and Onasch, T. B.: Collection efficiencies in an Aerodyne
708 Aerosol Mass Spectrometer as a function of particle phase for laboratory generated aerosols,
709 Aerosol Sci Tech, 42, 884-898, Doi 10.1080/02786820802356797, 2008.
710

711 Middlebrook, A. M., Bahreini, R., Jimenez, J. L., and Canagaratna, M. R.: Evaluation of
712 Composition-Dependent Collection Efficiencies for the Aerodyne Aerosol Mass Spectrometer
713 using Field Data, Aerosol Sci Tech, 46, 258-271, Doi 10.1080/02786826.2011.620041, 2012.
714

715 Milic, A., Mallet, M. D., Cravigan, L. T., Alroe, J., Ristovski, Z. D., Selleck, P., Lawson, S. J.,
716 Ward, J., Desservettaz, M. J., Paton-Walsh, C., Williams, L. R., Keywood, M. D., and Miljevic,
717 B.: Biomass burning and biogenic aerosols in northern Australia during the SAFIRED campaign,
718 Atmos. Chem. Phys., 17, 3945-3961, 10.5194/acp-17-3945-2017, 2017.

719

720 Mohr, C., Huffman, J. A., Cubison, M. J., Aiken, A. C., Docherty, K. S., Kimmel, J. R., Ulbrich,
721 I. M., Hannigan, M., and Jimenez, J. L.: Characterization of Primary Organic Aerosol Emissions
722 from Meat Cooking, Trash Burning, and Motor Vehicles with High-Resolution Aerosol Mass
723 Spectrometry and Comparison with Ambient and Chamber Observations, Environ Sci Technol,
724 43, 2443-2449, 10.1021/es8011518, 2009.
725

726 Murphy, B. N., Woody, M. C., Jimenez, J. L., Carlton, A. M. G., Hayes, P. L., Liu, S., Ng, N. L.,
727 Russell, L. M., Setyan, A., Xu, L., Young, J., Zaveri, R. A., Zhang, Q., and Pye, H. O. T.:
728 Semivolatile POA and parameterized total combustion SOA in CMAQv5.2: impacts on source
729 strength and partitioning, Atmos. Chem. Phys., 17, 11107-11133, 10.5194/acp-17-11107-2017,
730 2017a.
731

732 Murphy, B. N., Woody, M. C., Jimenez, J. L., Carlton, A. M. G., Hayes, P. L., Liu, S., Ng, N. L.,
733 Russell, L. M., Setyan, A., Xu, L., Young, J., Zaveri, R. A., Zhang, Q., and Pye, H. O. T.:
734 Semivolatile POA and parameterized total combustion SOA in CMAQv5.2: impacts on source
735 strength and partitioning, Atmos. Chem. Phys. Discuss., 2017, 1-44, 10.5194/acp-2017-193, 2017b.
736

737 Nah, T., McVay, R. C., Zhang, X., Boyd, C. M., Seinfeld, J. H., and Ng, N. L.: Influence of seed
738 aerosol surface area and oxidation rate on vapor wall deposition and SOA mass yields: a case study
739 with α-pinene ozonolysis, Atmos. Chem. Phys., 16, 9361-9379, 10.5194/acp-16-9361-2016, 2016.
740

741 Ng, N. L., Kroll, J. H., Chan, A. W. H., Chhabra, P. S., Flagan, R. C., and Seinfeld, J. H.: Secondary
742 organic aerosol formation from m-xylene, toluene, and benzene, Atmos. Chem. Phys., 7, 3909-
743 3922, 10.5194/acp-7-3909-2007, 2007.
744

745 Ng, N. L., Canagaratna, M. R., Zhang, Q., Jimenez, J. L., Tian, J., Ulbrich, I. M., Kroll, J. H.,
746 Docherty, K. S., Chhabra, P. S., Bahreini, R., Murphy, S. M., Seinfeld, J. H., Hildebrandt, L.,
747 Donahue, N. M., DeCarlo, P. F., Lanz, V. A., Prevot, A. S. H., Dinar, E., Rudich, Y., and Worsnop,
748 D. R.: Organic aerosol components observed in Northern Hemispheric datasets from Aerosol Mass
749 Spectrometry, Atmos Chem Phys, 10, 4625-4641, DOI 10.5194/acp-10-4625-2010, 2010.
750

751 Nolte, C. G., Appel, K. W., Kelly, J. T., Bhave, P. V., Fahey, K. M., Collett Jr, J. L., Zhang, L.,
752 and Young, J. O.: Evaluation of the Community Multiscale Air Quality (CMAQ) model v5.0
753 against size-resolved measurements of inorganic particle composition across sites in North
754 America, Geosci. Model Dev., 8, 2877-2892, 10.5194/gmd-8-2877-2015, 2015.
755

756 Odum, J. R., Hoffmann, T., Bowman, F., Collins, D., Flagan, R. C., and Seinfeld, J. H.:
757 Gas/Particle Partitioning and Secondary Organic Aerosol Yields, Environ Sci Technol, 30, 2580-
758 2585, 10.1021/es950943+, 1996.
759

760 Paatero, P., and Tapper, U.: Positive Matrix Factorization - a Nonnegative Factor Model with
761 Optimal Utilization of Error-Estimates of Data Values, Environmetrics, 5, 111-126, DOI
762 10.1002/env.3170050203, 1994.
763
764 Palm, B. B., de Sá, S. S., Day, D. A., Campuzano-Jost, P., Hu, W., Seco, R., Sjostedt, S. J., Park,
765 J. H., Guenther, A. B., Kim, S., Brito, J., Wurm, F., Artaxo, P., Thalman, R., Wang, J., Yee, L. D.,
766 Wernis, R., Isaacman-VanWertz, G., Goldstein, A. H., Liu, Y., Springston, S. R., Souza, R.,
767 Newburn, M. K., Alexander, M. L., Martin, S. T., and Jimenez, J. L.: Secondary organic aerosol
768 formation from ambient air in an oxidation flow reactor in central Amazonia, Atmos. Chem. Phys.
769 Discuss., 2017, 1-56, 10.5194/acp-2017-795, 2017.
770
771 Pathak, R. K., Stanier, C. O., Donahue, N. M., and Pandis, S. N.: Ozonolysis of alpha-pinene at
772 atmospherically relevant concentrations: Temperature dependence of aerosol mass fractions
773 (yields), J Geophys Res-Atmos, 112, Artn D03201
774 Doi 10.1029/2006jd007436, 2007.
775
776 Pye, H. O. T., Luecken, D. J., Xu, L., Boyd, C. M., Ng, N. L., Baker, K. R., Ayres, B. R., Bash, J.
777 O., Baumann, K., Carter, W. P. L., Edgerton, E., Fry, J. L., Hutzell, W. T., Schwede, D. B., and
778 Shepson, P. B.: Modeling the Current and Future Roles of Particulate Organic Nitrates in the
779 Southeastern United States, Environ Sci Technol, 49, 14195-14203, 10.1021/acs.est.5b03738,
780 2015.
781
782 Pye, H. O. T., Murphy, B. N., Xu, L., Ng, N. L., Carlton, A. G., Guo, H., Weber, R., Vasilakos,
783 P., Appel, K. W., Budisulistiorini, S. H., Surratt, J. D., Nenes, A., Hu, W., Jimenez, J. L., Isaacman-
784 VanWertz, G., Misztal, P. K., and Goldstein, A. H.: On the implications of aerosol liquid water
785 and phase separation for organic aerosol mass, Atmos. Chem. Phys., 17, 343-369, 10.5194/acp-
786 17-343-2017, 2017.
787
788 Reyes-Villegas, E., Priestley, M., Ting, Y. C., Haslett, S., Bannan, T., Le Breton, M., Williams, P.
789 I., Bacak, A., Flynn, M. J., Coe, H., Percival, C., and Allan, J. D.: Simultaneous aerosol mass
790 spectrometry and chemical ionisation mass spectrometry measurements during a biomass burning
791 event in the UK: insights into nitrate chemistry, Atmos. Chem. Phys., 18, 4093-4111, 10.5194/acp-
792 18-4093-2018, 2018.
793
794 Rindelaub, J. D., Borca, C. H., Hostetler, M. A., Slade, J. H., Lipton, M. A., Slipchenko, L. V.,
795 and Shepson, P. B.: The acid-catalyzed hydrolysis of an α-pinene-derived organic nitrate: kinetics,
796 products, reaction mechanisms, and atmospheric impact, Atmos. Chem. Phys., 16, 15425-15432,
797 10.5194/acp-16-15425-2016, 2016.
798
799 Robinson, N. H., Hamilton, J. F., Allan, J. D., Langford, B., Oram, D. E., Chen, Q., Docherty, K.,
800 Farmer, D. K., Jimenez, J. L., Ward, M. W., Hewitt, C. N., Barley, M. H., Jenkin, M. E., Rickard,
801 A. R., Martin, S. T., McFiggans, G., and Coe, H.: Evidence for a significant proportion of

802 Secondary Organic Aerosol from isoprene above a maritime tropical forest, Atmos Chem Phys,
803 11, 1039-1050, DOI 10.5194/acp-11-1039-2011, 2011.
804
805 Saha, P. K., and Grieshop, A. P.: Exploring Divergent Volatility Properties from Yield and
806 Thermodenuder Measurements of Secondary Organic Aerosol from α-Pinene Ozonolysis, Environ
807 Sci Technol, 10.1021/acs.est.6b00303, 2016.
808
809 Sanchez, J., Tanner, D. J., Chen, D., Huey, L. G., and Ng, N. L.: A new technique for the direct
810 detection of HO2 radicals using bromide chemical ionization mass spectrometry (Br-CIMS): initial
811 characterization, Atmos. Meas. Tech., 9, 3851-3861, 10.5194/amt-9-3851-2016, 2016.
812
813 Saunders, S. M., Jenkin, M. E., Derwent, R. G., and Pilling, M. J.: Protocol for the development
814 of the Master Chemical Mechanism, MCM v3 (Part A): tropospheric degradation of non-aromatic
815 volatile organic compounds, Atmos Chem Phys, 3, 161-180, 2003.
816
817 Shilling, J. E., Chen, Q., King, S. M., Rosenoern, T., Kroll, J. H., Worsnop, D. R., McKinney, K.
818 A., and Martin, S. T.: Particle mass yield in secondary organic aerosol formed by the dark
819 ozonolysis of alpha-pinene, Atmos Chem Phys, 8, 2073-2088, 2008.
820
821 Sun, Y., Du, W., Fu, P., Wang, Q., Li, J., Ge, X., Zhang, Q., Zhu, C., Ren, L., Xu, W., Zhao, J.,
822 Han, T., Worsnop, D. R., and Wang, Z.: Primary and secondary aerosols in Beijing in winter:
823 sources, variations and processes, Atmos. Chem. Phys., 16, 8309-8329, 10.5194/acp-16-8309-
824 2016, 2016.
825
826 Tasoglou, A., and Pandis, S. N.: Formation and chemical aging of secondary organic aerosol
827 during the β-caryophyllene oxidation, Atmos. Chem. Phys., 15, 6035-6046, 10.5194/acp-15-6035-
828 2015, 2015.
829
830 Tuet, W. Y., Chen, Y., Xu, L., Fok, S., Gao, D., Weber, R. J., and Ng, N. L.: Chemical oxidative
831 potential of secondary organic aerosol (SOA) generated from the photooxidation of biogenic and
832 anthropogenic volatile organic compounds, Atmos. Chem. Phys., 17, 839-853, 10.5194/acp-17-
833 839-2017, 2017.
834
835 Ulbrich, I. M., Canagaratna, M. R., Zhang, Q., Worsnop, D. R., and Jimenez, J. L.: Interpretation
836 of organic components from Positive Matrix Factorization of aerosol mass spectrometric data,
837 Atmos. Chem. Phys., 9, 2891-2918, 2009a.
838
839 Ulbrich, I. M., Canagaratna, M. R., Zhang, Q., Worsnop, D. R., and Jimenez, J. L.: Interpretation
840 of organic components from Positive Matrix Factorization of aerosol mass spectrometric data,
841 Atmos. Chem. Phys., 9, 2891-2918, 10.5194/acp-9-2891-2009, 2009b.
842

Vaden, T. D., Imre, D., Beránek, J., Shrivastava, M., and Zelenyuk, A.: Evaporation kinetics and phase of laboratory and ambient secondary organic aerosol, Proceedings of the National Academy of Sciences, 108, 2190-2195, 10.1073/pnas.1013391108, 2011.

Xu, L., Kollman, M. S., Song, C., Shilling, J. E., and Ng, N. L.: Effects of NOx on the Volatility of Secondary Organic Aerosol from Isoprene Photooxidation, Environ Sci Technol, 48, 2253-2262, 10.1021/es404842g, 2014.

Xu, L., Guo, H., Boyd, C. M., Klein, M., Bougiatioti, A., Cerully, K. M., Hite, J. R., Isaacman-VanWertz, G., Kreisberg, N. M., Knote, C., Olson, K., Koss, A., Goldstein, A. H., Hering, S. V., de Gouw, J., Baumann, K., Lee, S.-H., Nenes, A., Weber, R. J., and Ng, N. L.: Effects of anthropogenic emissions on aerosol formation from isoprene and monoterpenes in the southeastern United States, Proceedings of the National Academy of Sciences, 112, 37-42, 10.1073/pnas.1417609112, 2015a.

Xu, L., Suresh, S., Guo, H., Weber, R. J., and Ng, N. L.: Aerosol characterization over the southeastern United States using high-resolution aerosol mass spectrometry: spatial and seasonal variation of aerosol composition and sources with a focus on organic nitrates, Atmos. Chem. Phys., 15, 7307-7336, 10.5194/acp-15-7307-2015, 2015b.

Xu, L., Guo, H., Weber, R. J., and Ng, N. L.: Chemical Characterization of Water-Soluble Organic Aerosol in Contrasting Rural and Urban Environments in the Southeastern United States, Environ Sci Technol, 51, 78-88, 10.1021/acs.est.6b05002, 2017.

Xu, W., Han, T., Du, W., Wang, Q., Chen, C., Zhao, J., Zhang, Y., Li, J., Fu, P., Wang, Z., Worsnop, D. R., and Sun, Y.: Effects of Aqueous-Phase and Photochemical Processing on Secondary Organic Aerosol Formation and Evolution in Beijing, China, Environ Sci Technol, 10.1021/acs.est.6b04498, 2016.

Yu, J., Cocker, D. R., Griffin, R. J., Flagan, R. C., and Seinfeld, J. H.: Gas-Phase Ozone Oxidation of Monoterpenes: Gaseous and Particulate Products, J Atmos Chem, 34, 207-258, 10.1023/a:1006254930583, 1999.

Yu, L., Smith, J., Laskin, A., Anastasio, C., Laskin, J., and Zhang, Q.: Chemical characterization of SOA formed from aqueous-phase reactions of phenols with the triplet excited state of carbonyl and hydroxyl radical, Atmos. Chem. Phys., 14, 13801-13816, 10.5194/acp-14-13801-2014, 2014.

Zhang, Q., Jimenez, J. L., Canagaratna, M. R., Ulbrich, I. M., Ng, N. L., Worsnop, D. R., and Sun, Y. L.: Understanding atmospheric organic aerosols via factor analysis of aerosol mass spectrometry: a review, Anal Bioanal Chem, 401, 3045-3067, DOI 10.1007/s00216-011-5355-y, 2011.

885 Zhang, X., McVay, R. C., Huang, D. D., Dalleska, N. F., Aumont, B., Flagan, R. C., and Seinfeld,
886 J. H.: Formation and evolution of molecular products in α-pinene secondary organic aerosol,
887 Proceedings of the National Academy of Sciences, 112, 14168-14173, 10.1073/pnas.1517742112,
888 2015.
889
890 Zhang, Y., Tang, L., Croteau, P. L., Favez, O., Sun, Y., Canagaratna, M. R., Wang, Z., Couvidat,
891 F., Albinet, A., Zhang, H., Sciare, J., Prévôt, A. S. H., Jayne, J. T., and Worsnop, D. R.: Field
892 characterization of the PM2.5 Aerosol Chemical Speciation Monitor: insights into the composition,
893 sources and processes of fine particles in Eastern China, Atmos. Chem. Phys. Discuss., 2017, 1-
894 52, 10.5194/acp-2017-233, 2017.
895
896

897

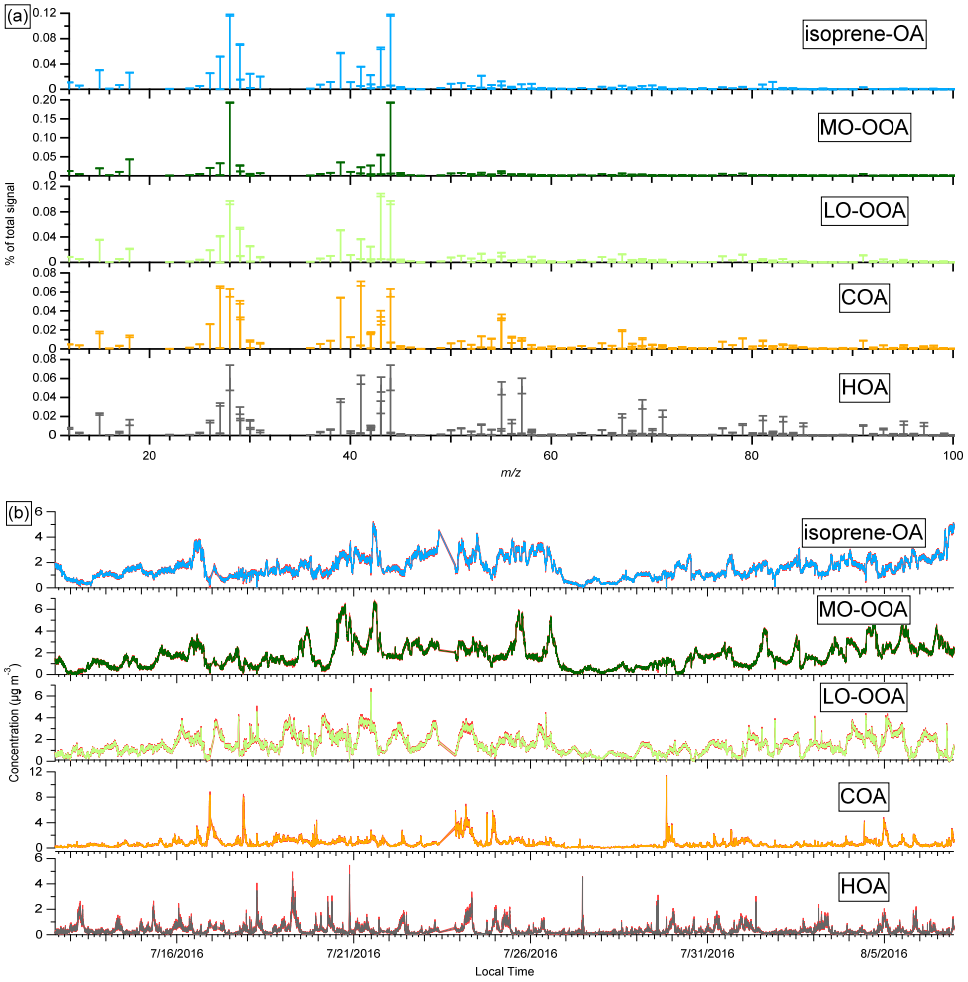

898

899 Fig. S1. PMF results from bootstrapping analysis. (a) Average mass spectra (sticks) with 1-σ error
900 bars (caps). (b) Average time series and 1-σ error bars (red).

901

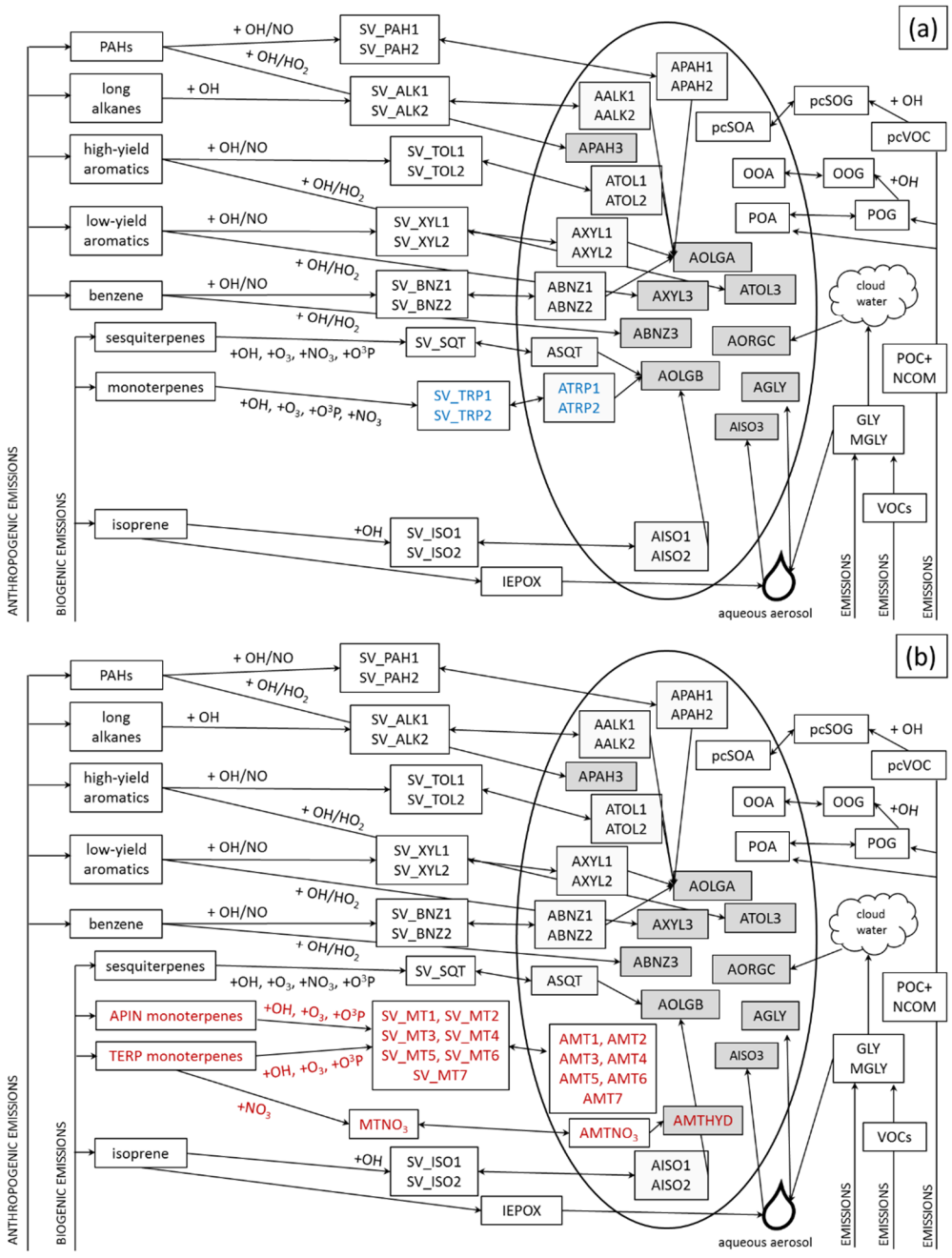

Fig. S2. Schematic of SOA treatment in (a) default simulation (v5.2) and (b) updated simulation in CMAQ. See Pye et al. (2017) for a description of the traditional and aqueous aerosol SOA systems. See Murphy et al. (2017) for a description of the semivolatile POA (POA, POG), oxidized POA vapors (OOA, OOG) and potential SOA from combustion sources (pcSOA) system. See Pye et al. (2015) for MTNO3 formation and hydrolysis. In the default simulation, species in blue were not formed in the updated simulation. In the updated simulation, species in red are different from the default simulation.

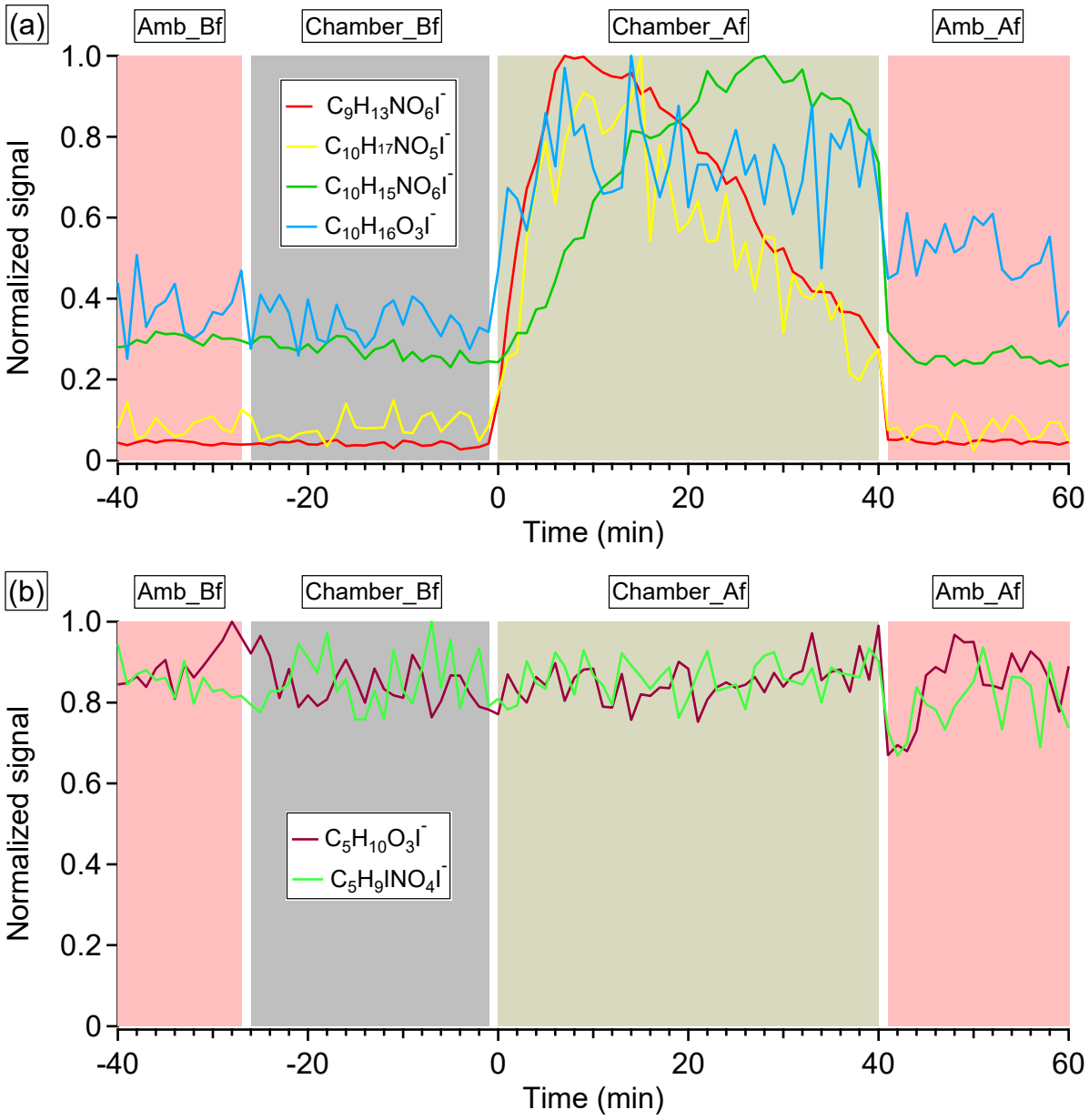

Fig. S3. Time series of gas-phase species detected by HR-ToF-CIMS using I^- as reagent ion in experiment ap_0718_1. Panel (a) includes four major known α-pinene oxidation products. Panel (b) includes two major known isoprene oxidation products. The signal is normalized to I^- and then normalized to the maximum signal in the time window shown in the figure.

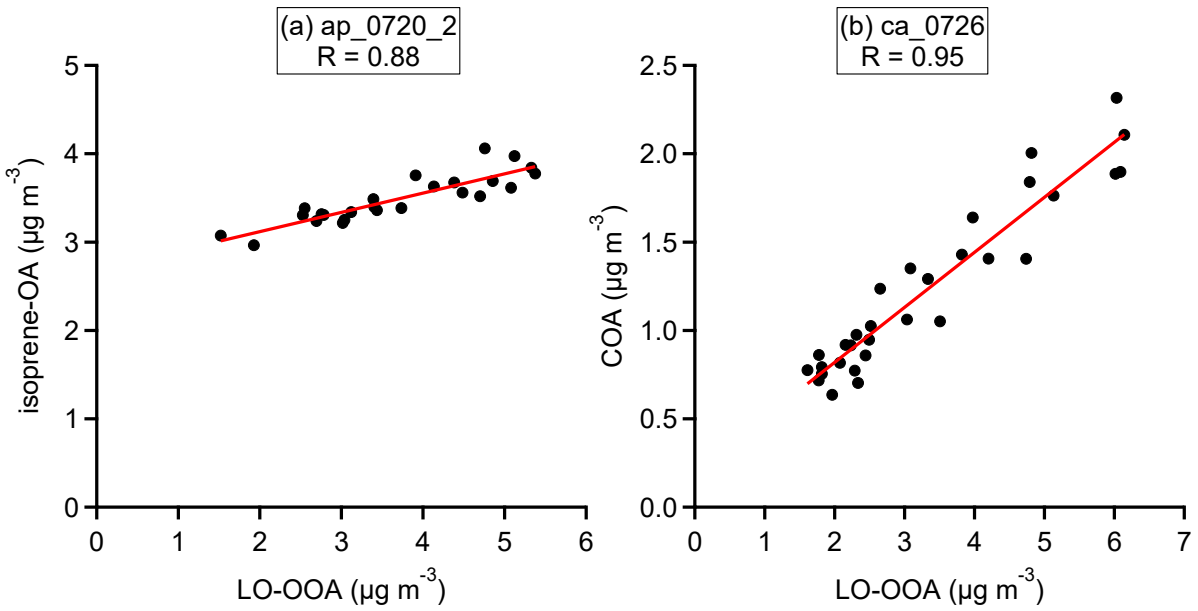

917

918 Fig. S4. (a) The correlation between isoprene-OA and LO-OOA in the "Chamber_Af" period of
919 one α-pinene perturbation experiment (i.e., ap_0720_2). (b) The correlation between COA and
920 LO-OOA in the "Chamber_Af" period of one β-caryophyllene experiment (i.e., ca_0726).

921

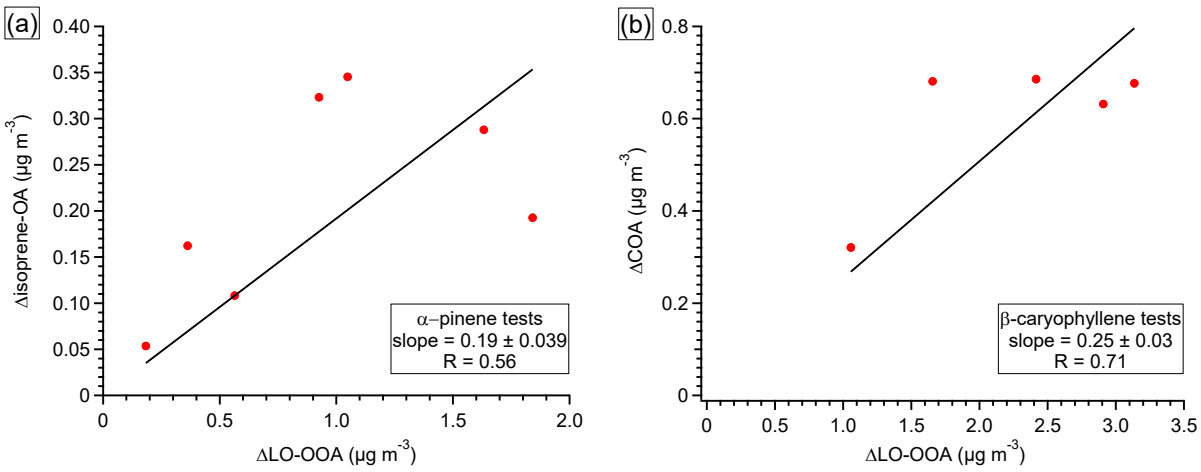

922

923 Fig. S5. (a) The relationship between isoprene-OA enhancement and LO-OOA enhancement in α-
924 pinene perturbation experiments. (b) The relationship between COA enhancement and LO-OOA
925 enhancement in β-caryophyllene perturbation experiments. The slopes are from orthogonal fit. The
926 R is from least square fit. The intercepts are forced to be zero. In α-pinene experiments, isoprene-
927 OA enhancement is 19% of LO-OOA enhancement. Thus, every 1 μg m^{-3} SOA is formed from α-
928 pinene oxidation, 0.16 μg m^{-3} [i.e., 0.19/(1+0.19)] is apportioned into isoprene-OA factor and the
929 rest to LO-OOA factor.

930

931

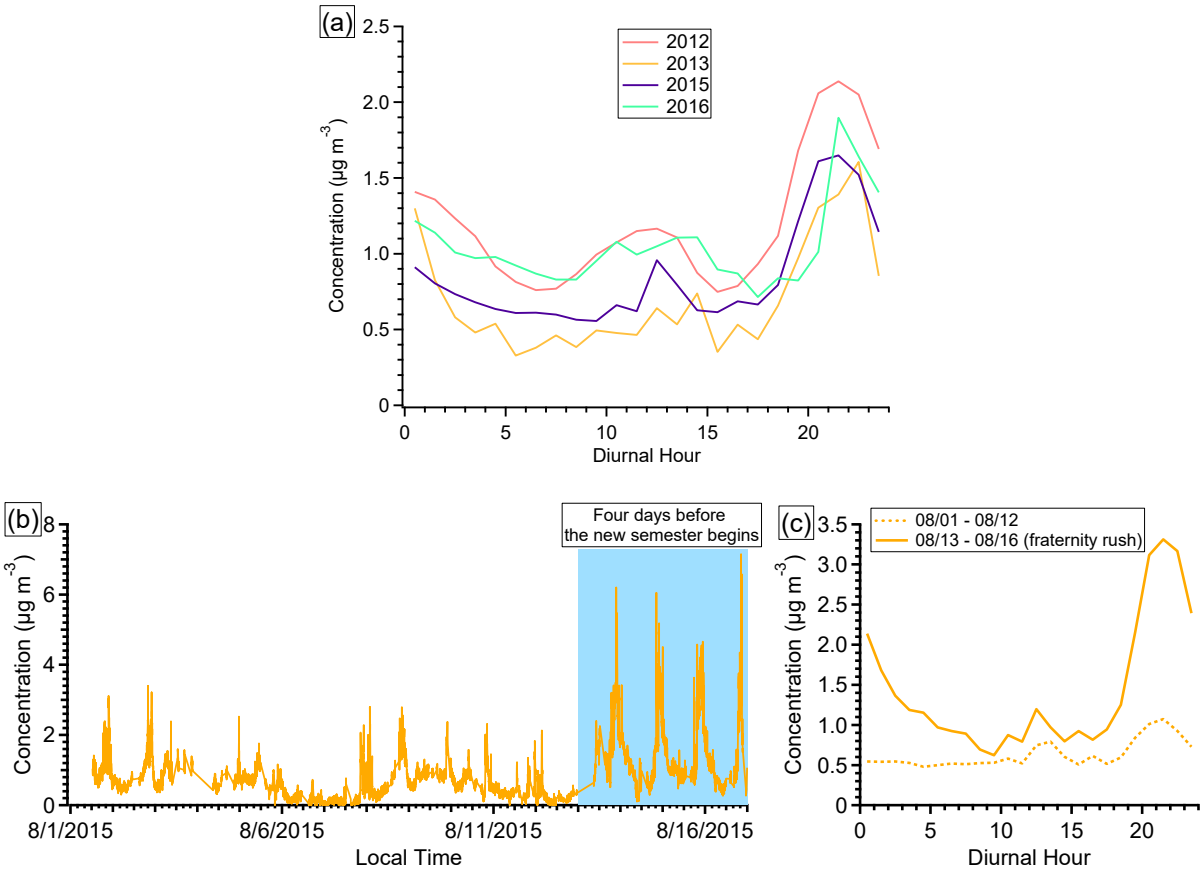

932

933 Fig. S6. (a) The diurnal trends of COA in ambient measurements conducted in different years
934 (2012 to 2016). (b) Time series of COA in 2015 measurements. (c) Diurnal trends of COA during
935 two periods of measurements in 2015 (08/01-08/21 and 08/13-08/16).

936

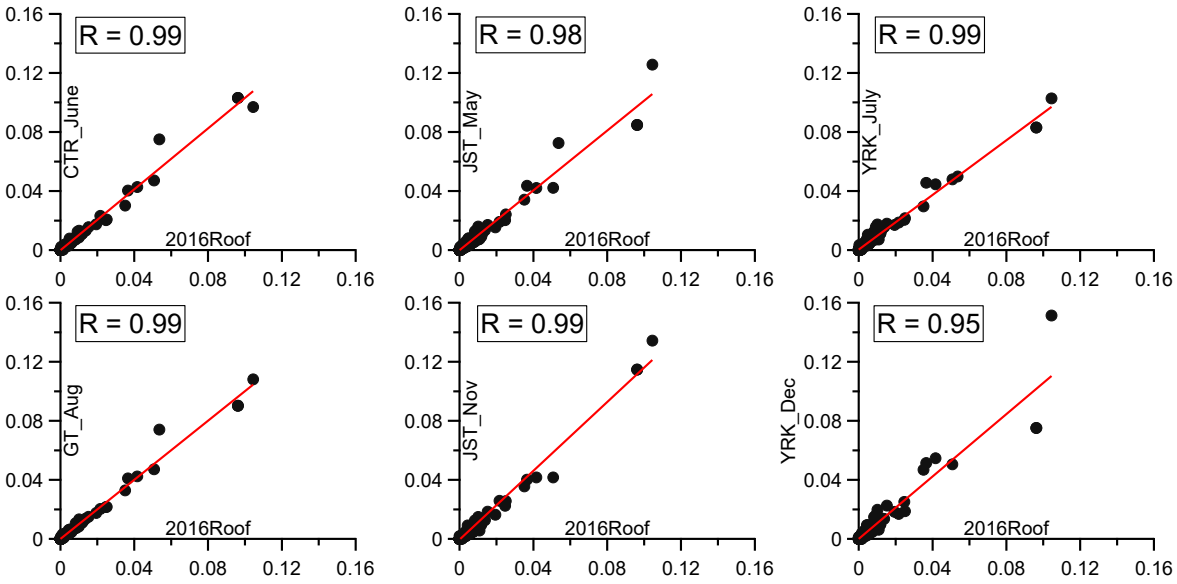

937

938 Fig. S7. The correlation plot between the mass spectrum of LO-OOA for 2016 rooflab perturbation
939 study and the LO-OOA obtained in other six ambient datasets in the southeastern U.S.

940

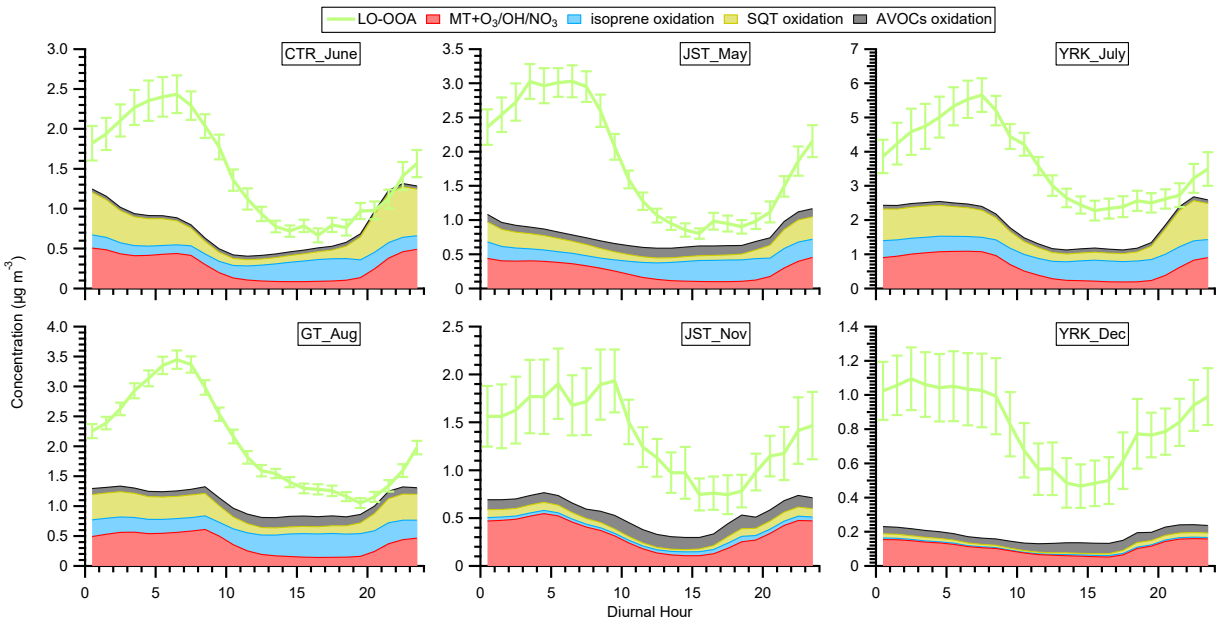

941

942 Fig. S8. The diurnal trends of LO-OOA and all fresh SOA (including isoprene (Odum two-product
943 representation), monoterpenes, sesquiterpenes, and anthropogenic VOCs) at different sampling
944 sites in the southeastern U.S. in the default CMAQv5.2 simulation. The error bars indicate the
945 standard error.

946

947

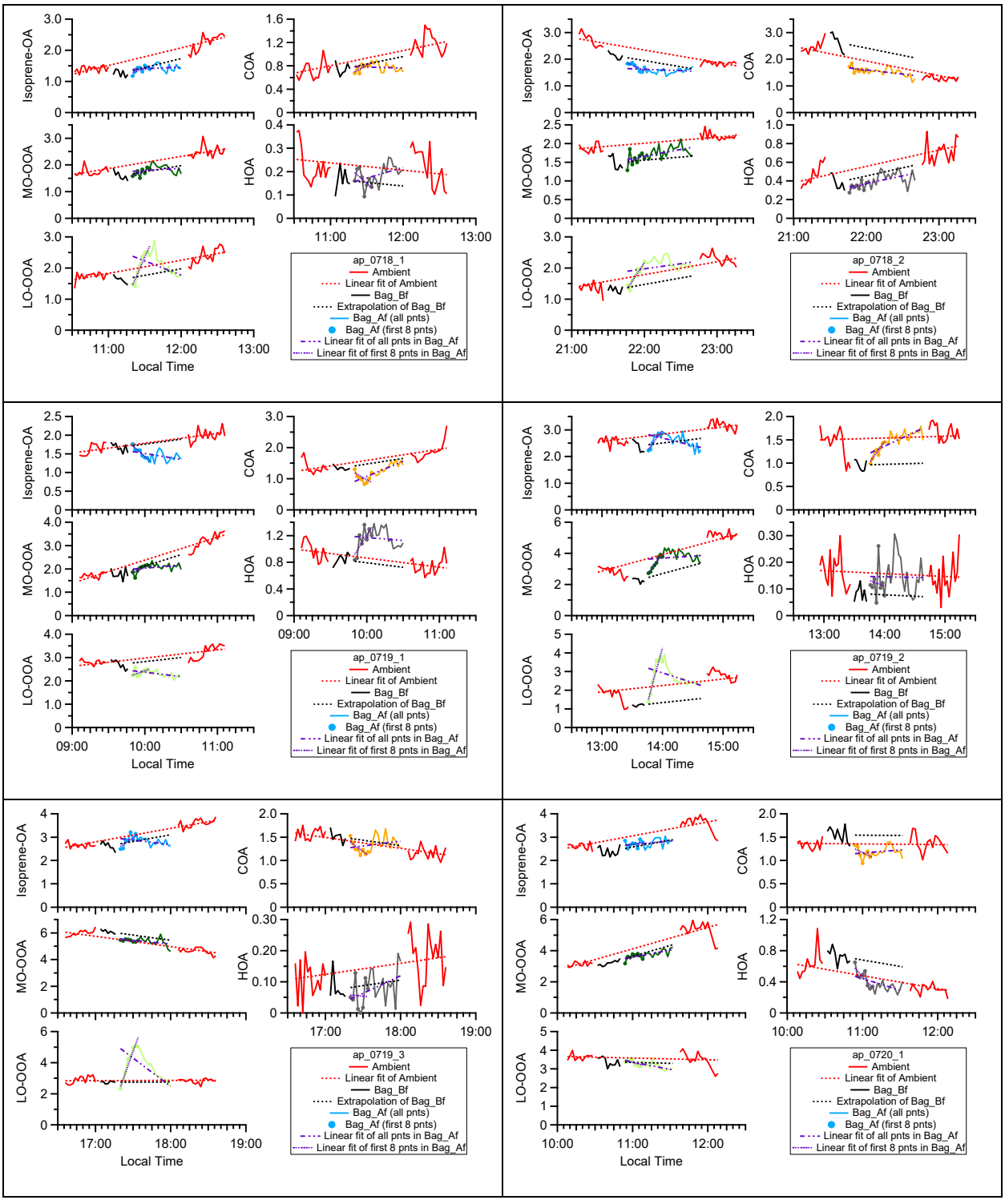
Isoprene-OA
COA
MO-OOA
HOA
LO-OOA
Local Time
ap_0718_1
ap_0718_2
ap_0719_1
ap_0719_2
ap_0719_3
ap_0720_1
Ambient
Linear fit of Ambient
Bag_Bf
Extrapolation of Bag_Bf
Bag_Af (all pnts)
Bag_Af (first 8 pnts)
Linear fit of all pnts in Bag_Af
Linear fit of first 8 pnts in Bag_Af

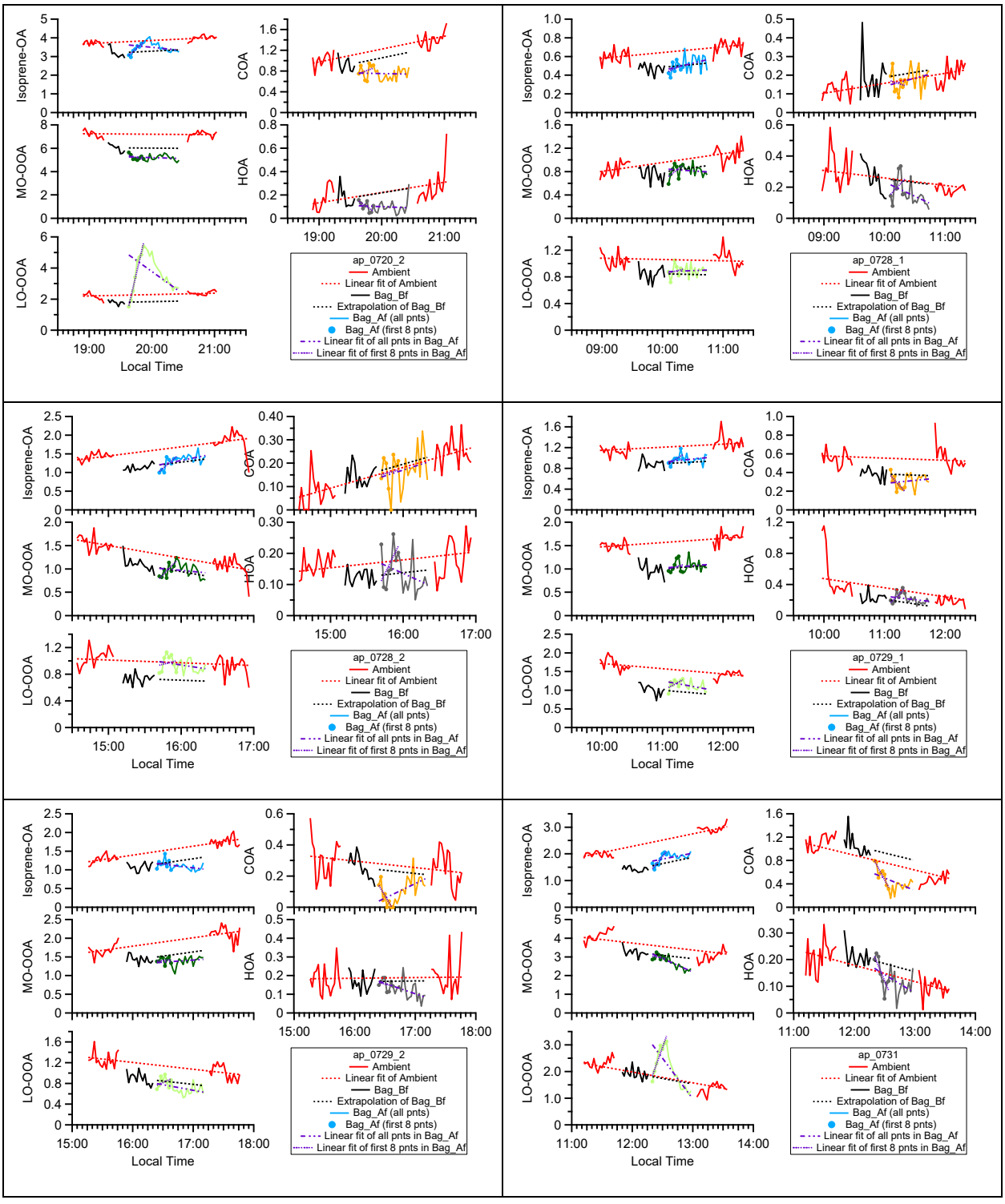
Isoprene-OA
MO-OOA
LO-OOA
COA
HOA
Local Time
ap_0720_2
ap_0728_1
ap_0728_2
ap_0729_1
ap_0729_2
ap_0731
Ambient
Linear fit of Ambient
Bag_Bf
Extrapolation of Bag_Bf
Bag_Af (all pnts)
Bag_Af (first 8 pnts)
Linear fit of all pnts in Bag_Af
Linear fit of first 8 pnts in Bag_Af

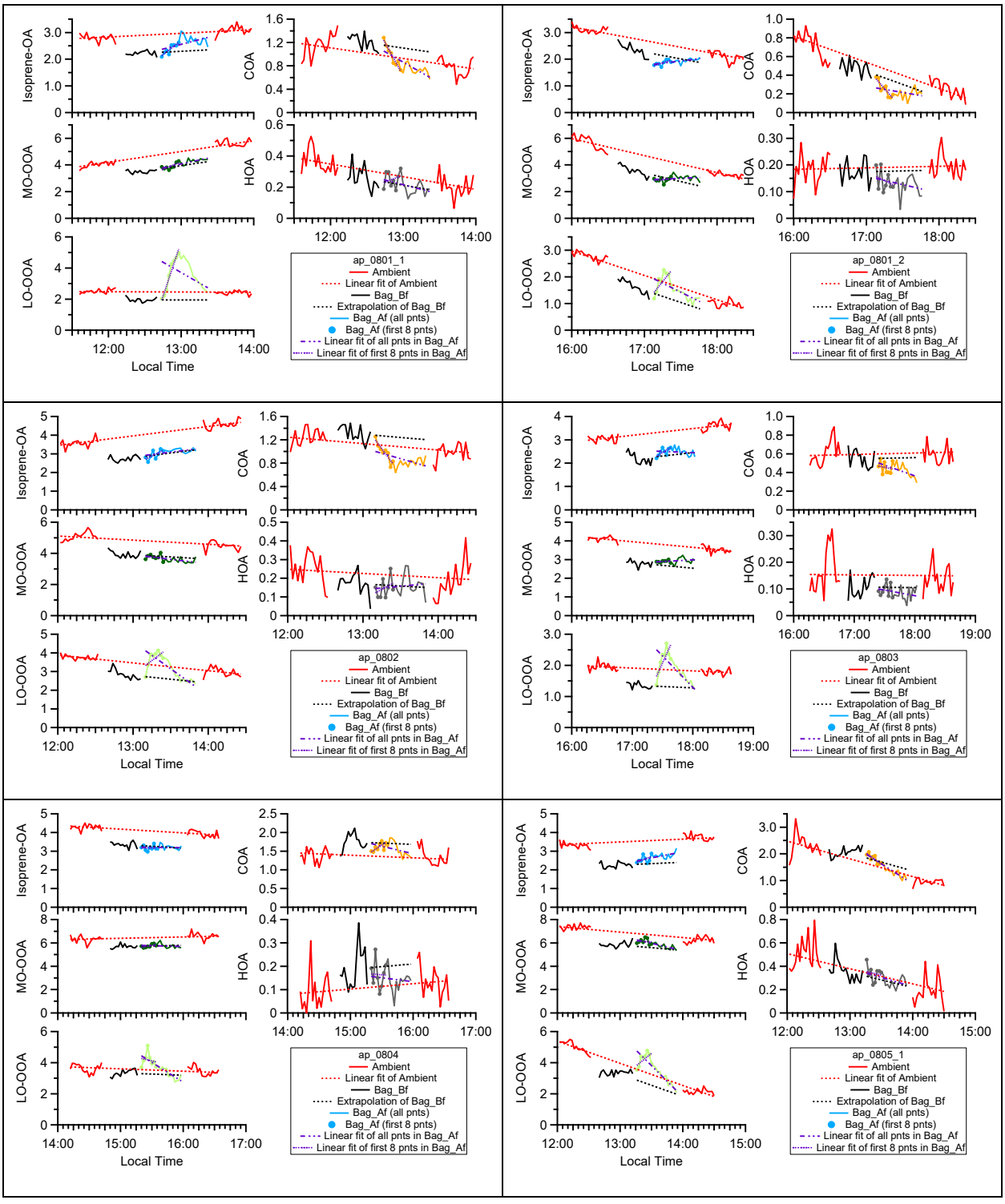
Isoprene-OA
COA
MO-OOA
HOA
LO-OOA
Local Time
ap_0801_1
ap_0801_2
ap_0802
ap_0803
ap_0804
ap_0805_1
Ambient
Linear fit of Ambient
Bag_Bf
Extrapolation of Bag_Bf
Bag_Af (all pnts)
Bag_Af (first 8 pnts)
Linear fit of all pnts in Bag_Af
Linear fit of first 8 pnts in Bag_Af

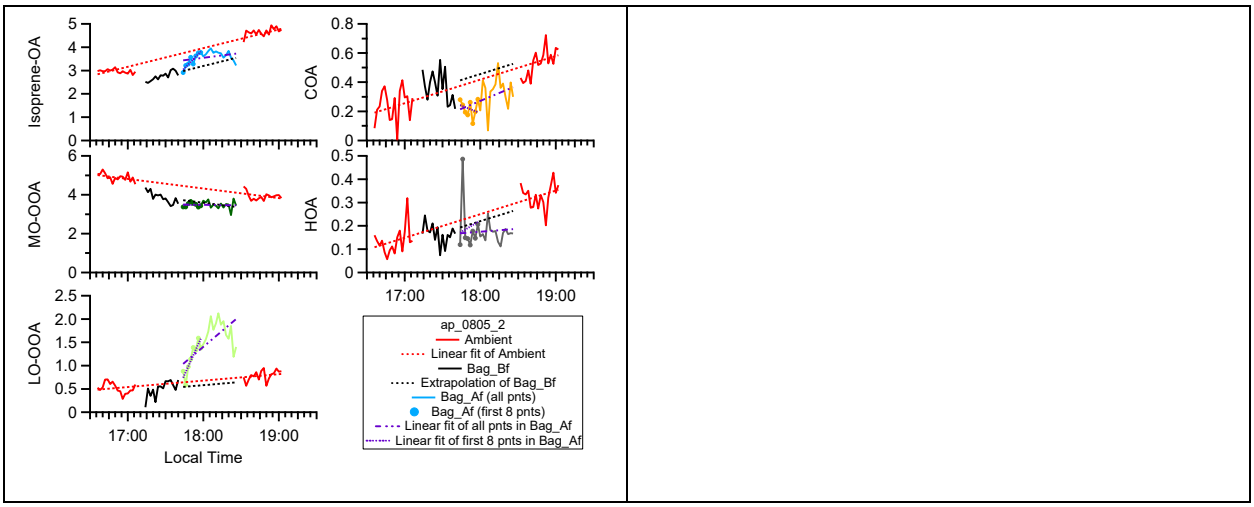

948 Fig. S9(a). Time series of OA factors in each α-pinene experiment.

949

950

951

952

953

954

955

956

957

958

959

960

961

962

963

964

965

966

967

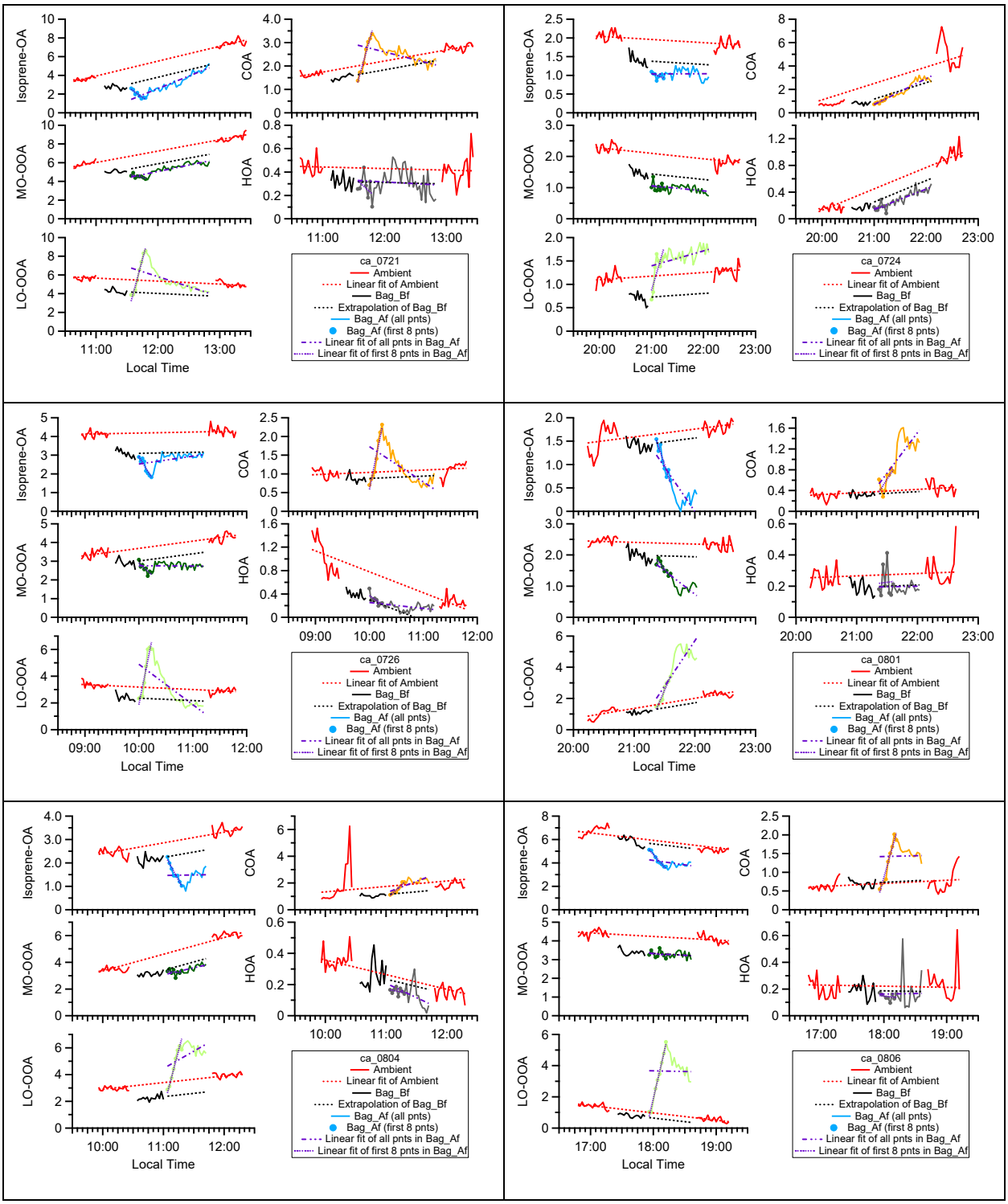

968 Fig. S9(b). Time series of OA factors in each β-caryophyllene experiment.

969

970

971

972

973 Fig. S10. The average mass fraction of OA factors in Amb_Bf and Chamber_Bf periods in α-
974 pinene experiments. The error bars represent the standard deviation. For most experiments, the
975 average mass fractions in these two periods are not statistically significantly different, suggesting
976 that the overall OA compositions are not statistically significantly different between two periods.

977

978

979

980

981

982

983

α-pinene experiments

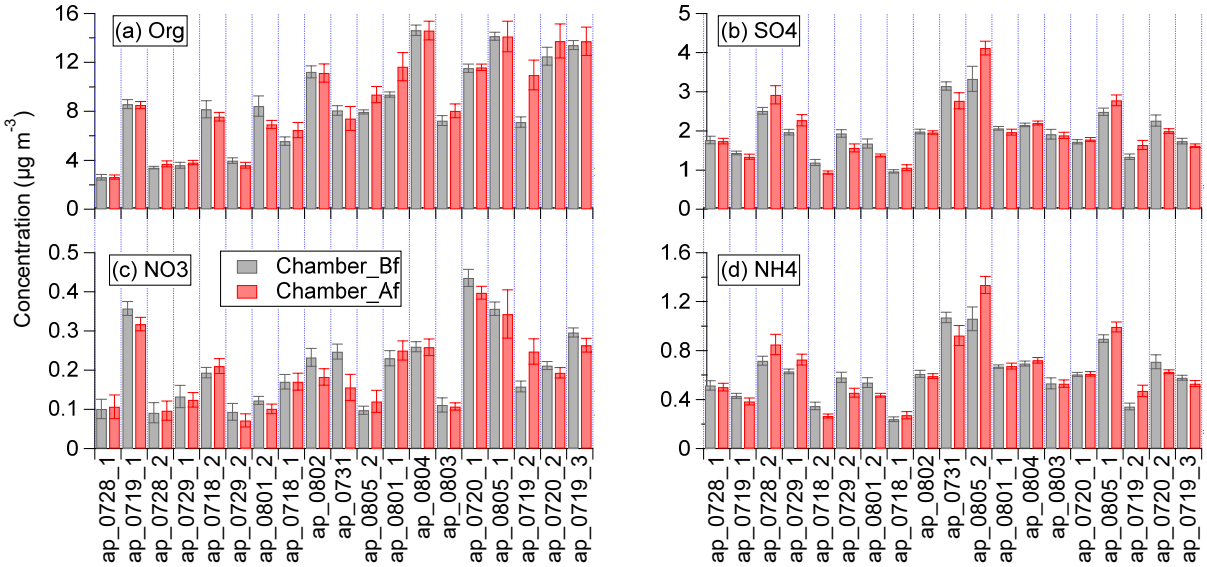

β-caryophyllene experiments

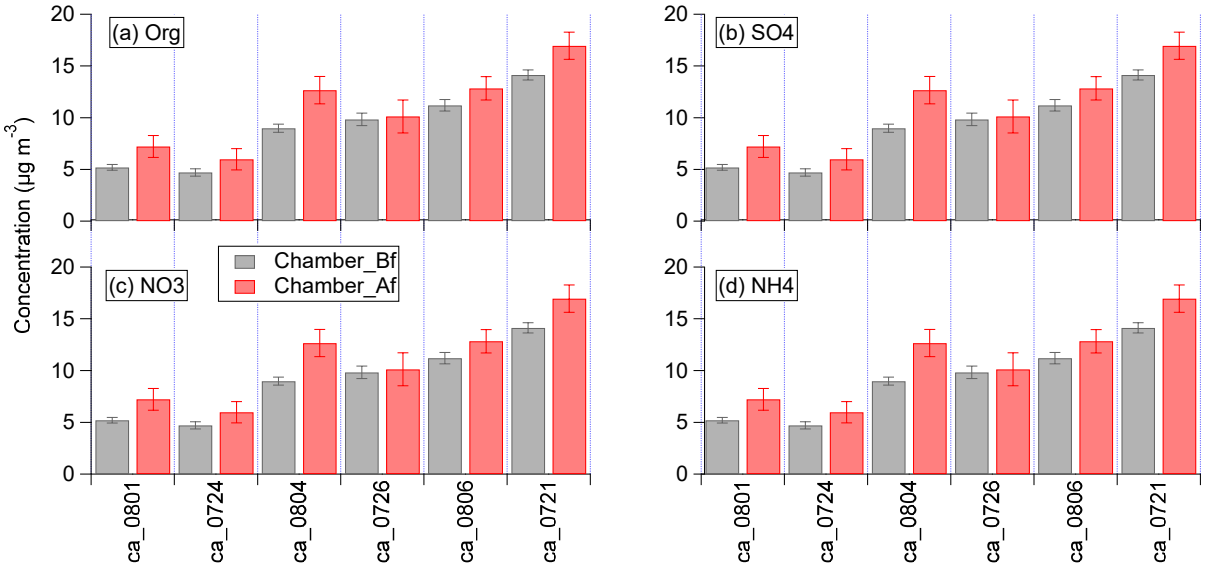

Fig. S11. The comparison of (a) Org, (b) SO_4, (c) NO_3, and (d) NH_4 concentrations between "Chamber_Bf" and "Chamber_Af" for α-pinene and β-caryophyllene perturbation experiments. Note that the concentrations reported in these figures are simply from average over each period, without any statistical analysis discussed in Appendix A. Thus, the differences between two periods are highly affected by ambient variation.

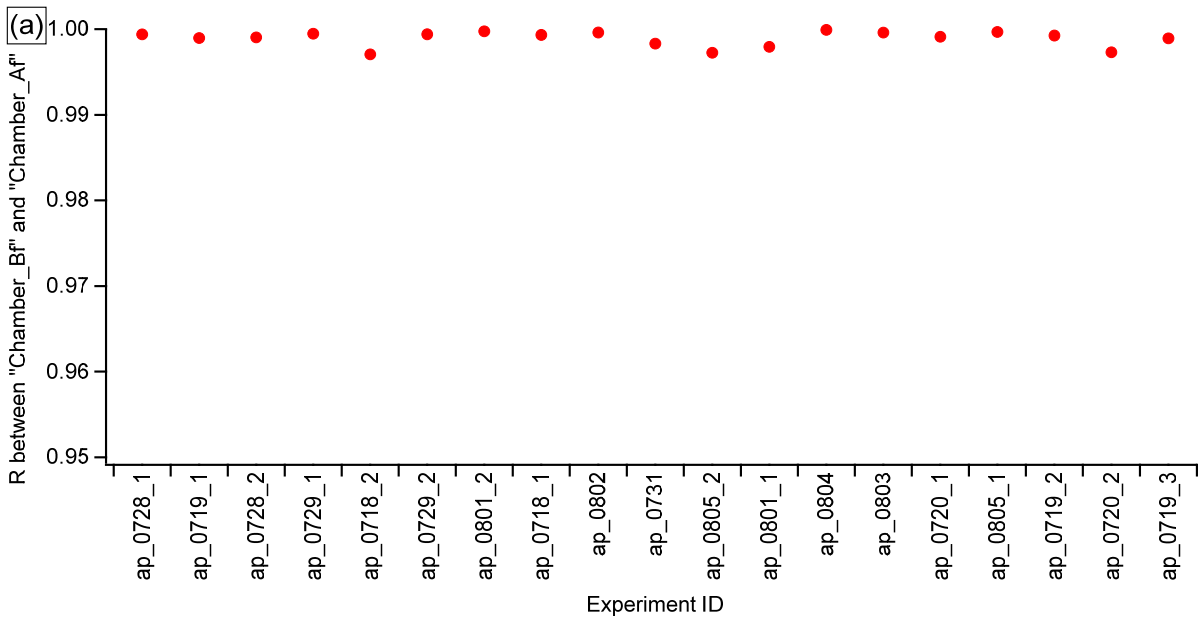

993

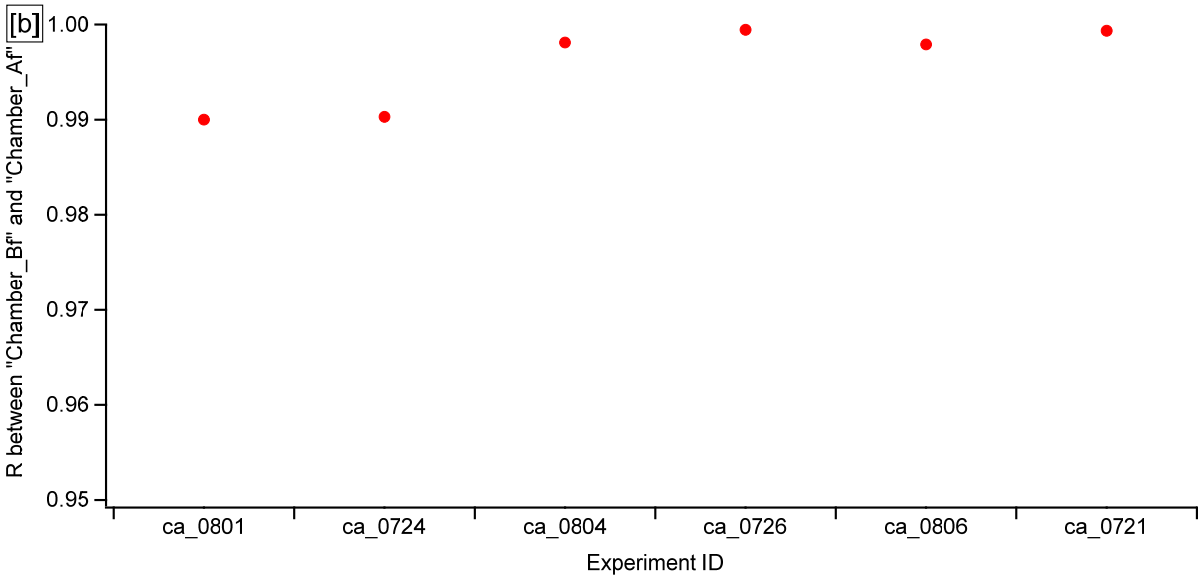

994

995 Fig. S12. The correlation coefficient by comparing the OA mass spectra between “Chamber_Bf”
996 and “Chamber_Af” in (a) α-pinene and (b) β-caryophyllene perturbation experiments.

997

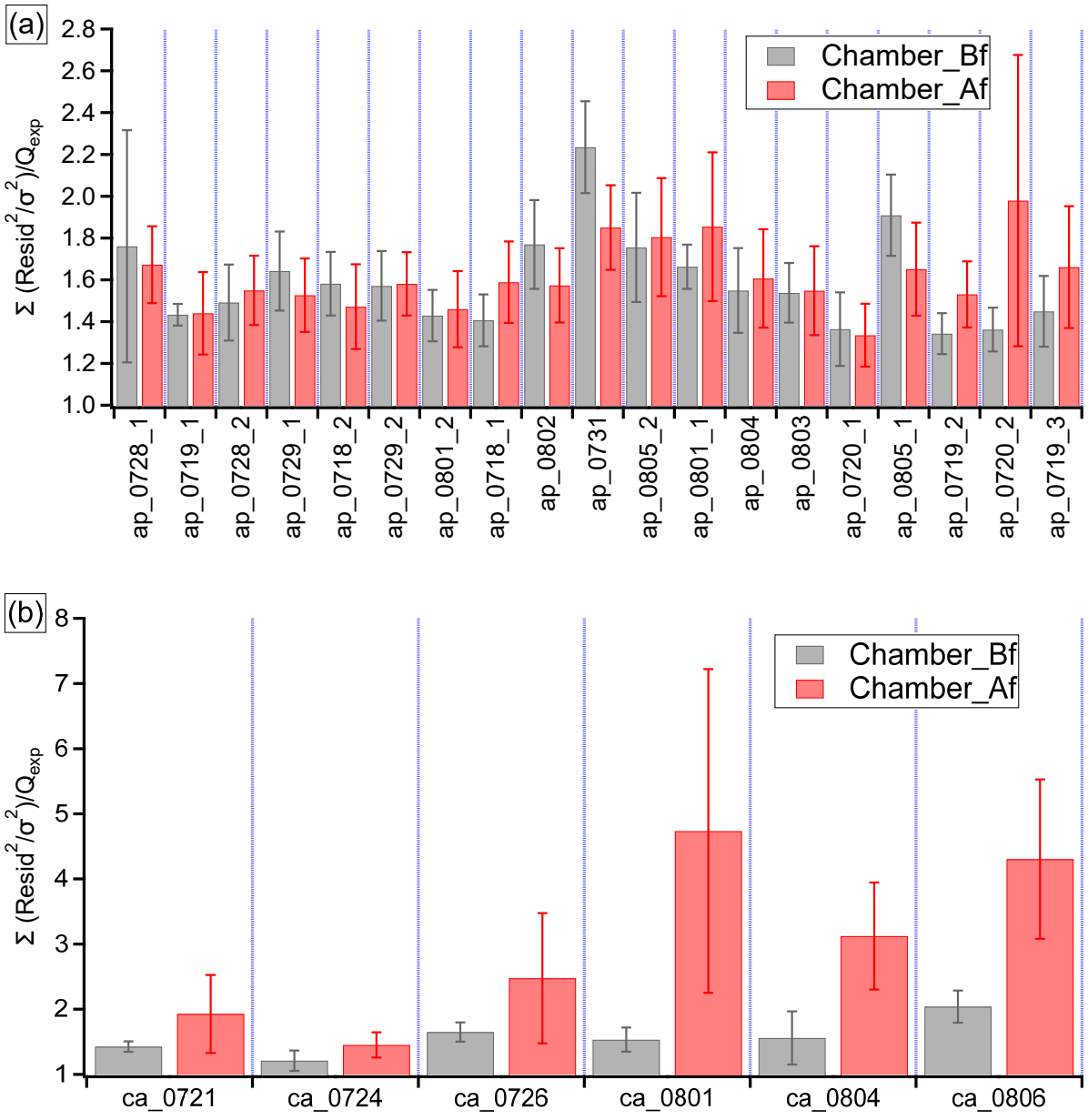

998

999 Fig. S13. The PMF residual (Q/Q_{exp}) during "Chamber_Bf" and "Chamber_Af" periods for (a) α-

1000 pinene and (b) β-caryophyllene perturbation experiments.

1001

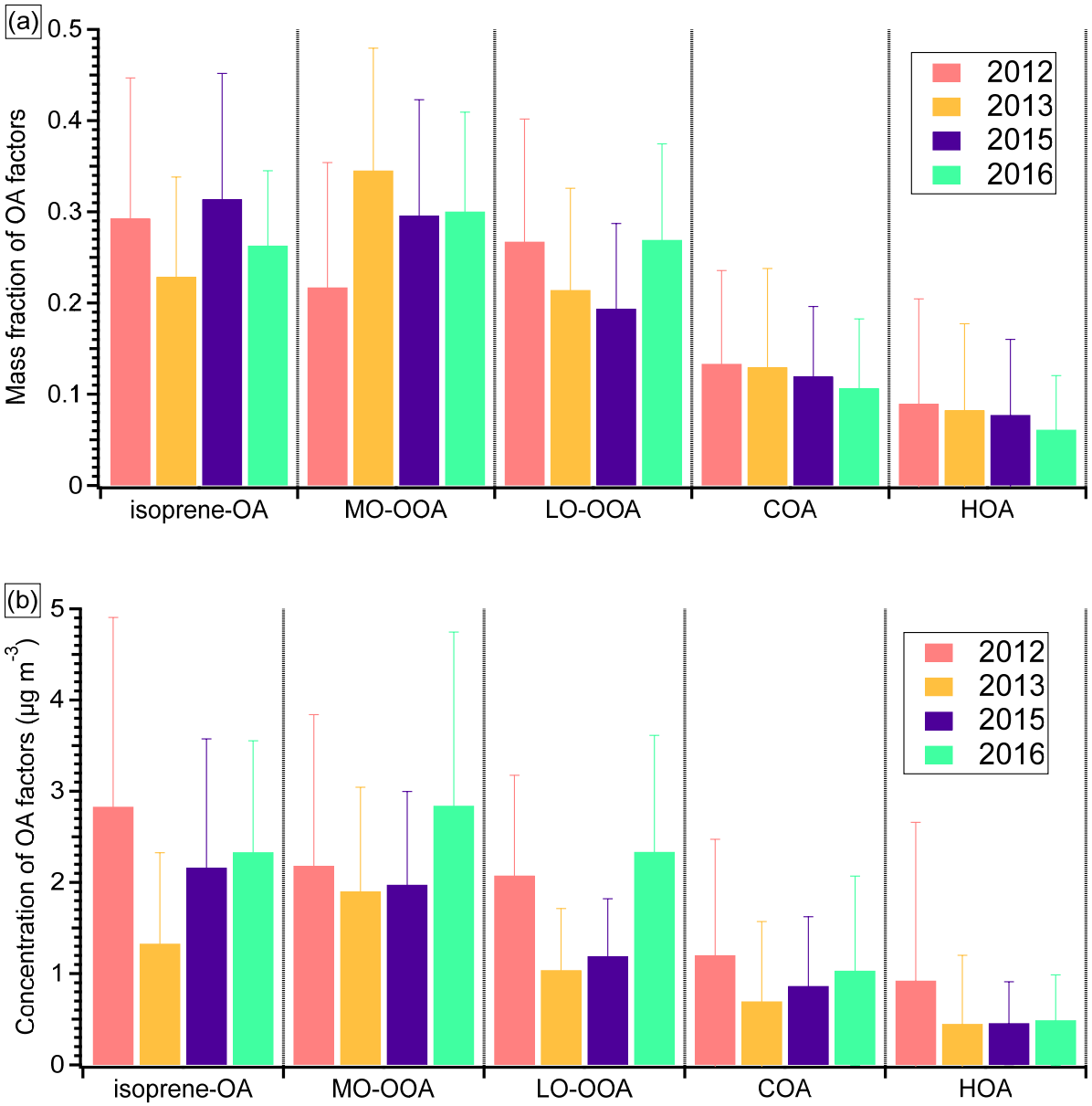

1002

1003

1004 Fig. S14. The mass fraction of OA factors in ambient measurements conducted in different years
1005 (2012 to 2016).

1006

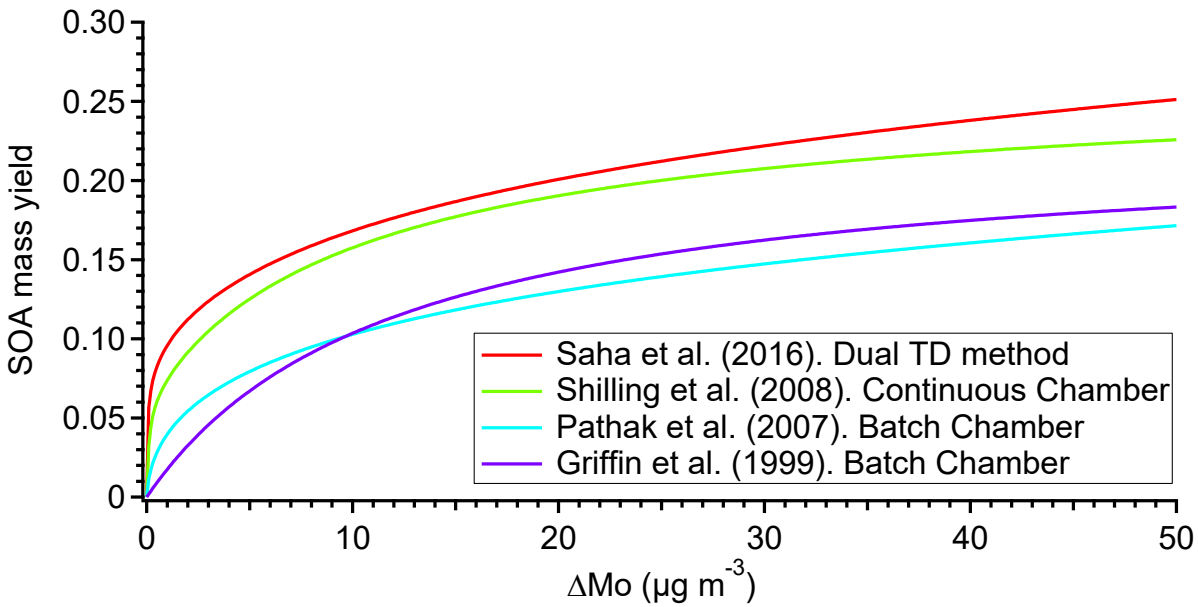

1007

1008 Fig. S15. Comparison of the SOA mass yields of α-pinene ozonolysis in the literature. SOA
1009 density of 1 g cm^{-3} is used in all studies to facilitate comparison. Note that in Saha et al. (2016),
1010 the SOA concentration is required to calculate the SOA yield parameterizations. The yields with
1011 445 μg m^{-3} aerosol loading (column *i* of Table 1 in Saha et al.) are reported in this study.

1012

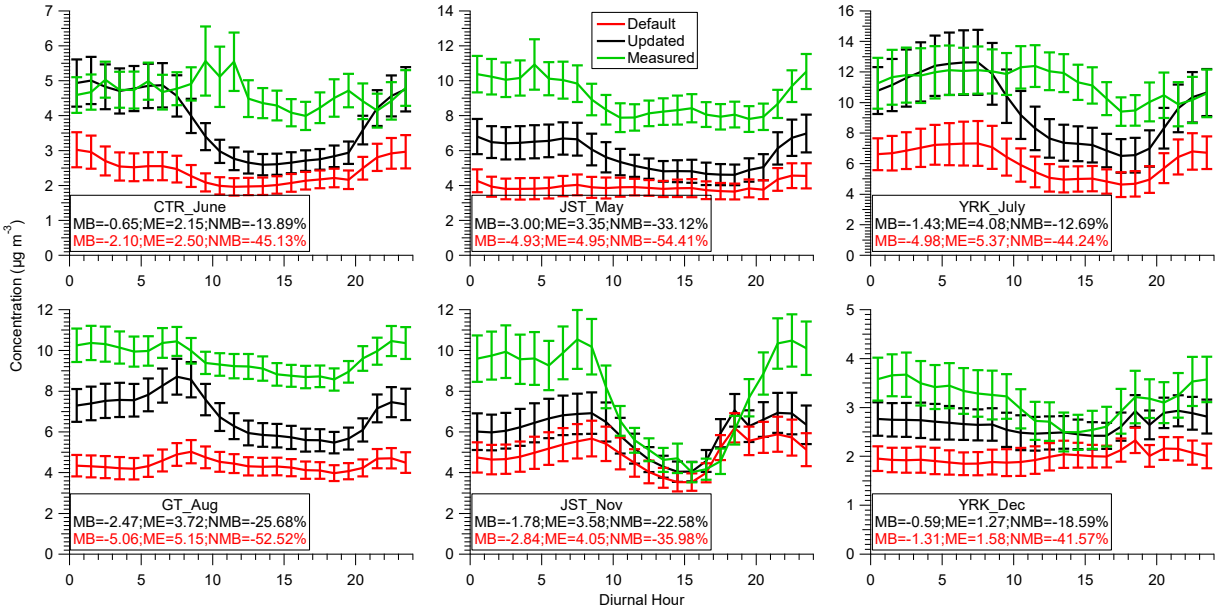

Fig. S16. The diurnal trends of AMS measured OA and CMAQ predicted OA mass concentration (PM_1) in both default and updated simulations. Mean bias (MB), mean error (ME), normalized mean bias (NMB) are shown in each panel.

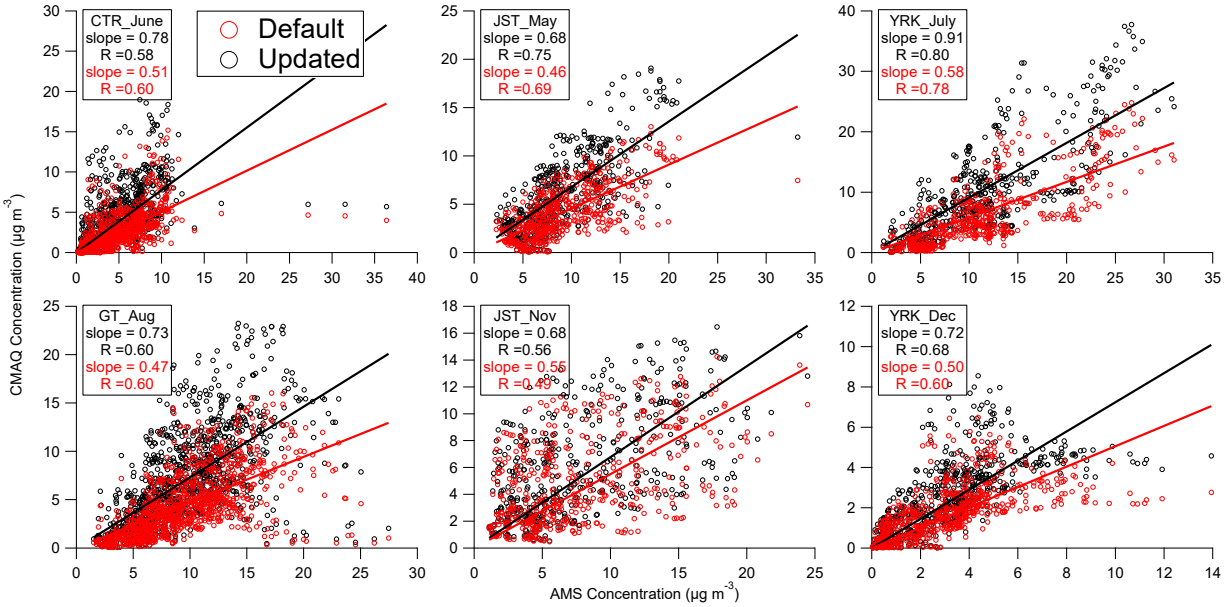

1018

1019 Fig. S17. The scatter plots of AMS measured OA and CMAQ predicted OA mass concentration in

1020 both default and updated simulations. The slopes and R are obtained by least square fit.

1021

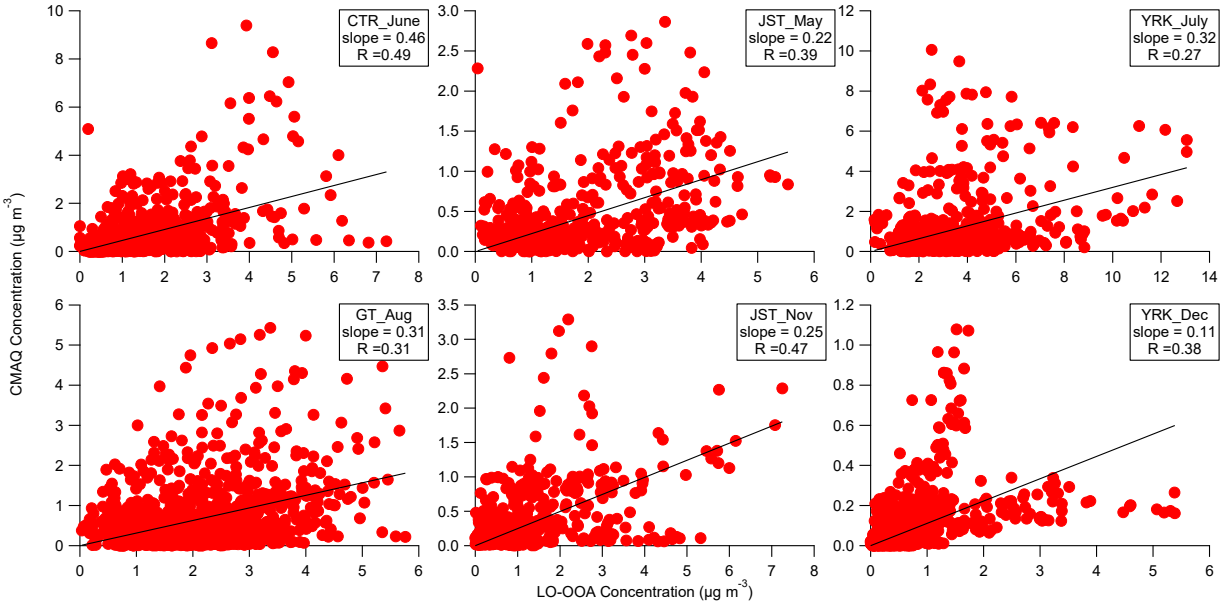

1022

1023 Fig. S18. The scatter plots of LO-OOA and CMAQ predicted SOA mass concentration from
1024 monoterpenes and sesquiterpenes in the default simulation at different sampling sites in the
1025 southeastern U.S. The slopes and R are obtained by least square fit. The intercepts are forced to be
1026 zero.

1027

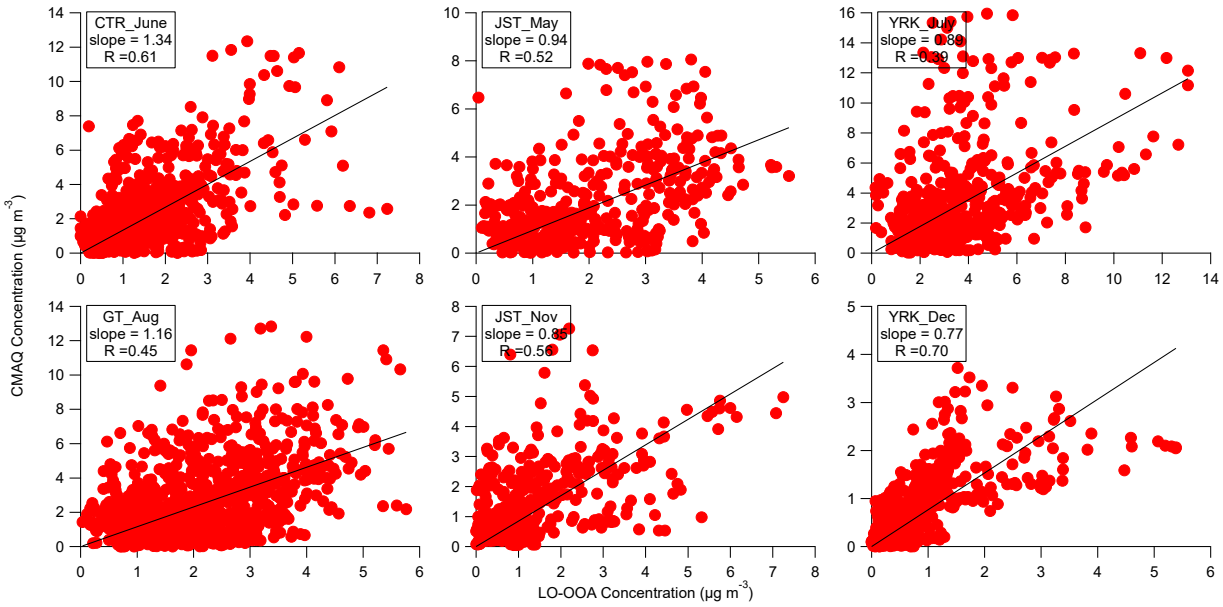

1028

1029 Fig. S19. The scatter plot between LO-OOA and modeled SOA mass concentration from
1030 monoterpenes and sesquiterpenes in updated simulation at different sampling sites in the
1031 southeastern U.S. The slope sand R are obtained from the least square fit. The intercepts are forced
1032 to be zero.

1033

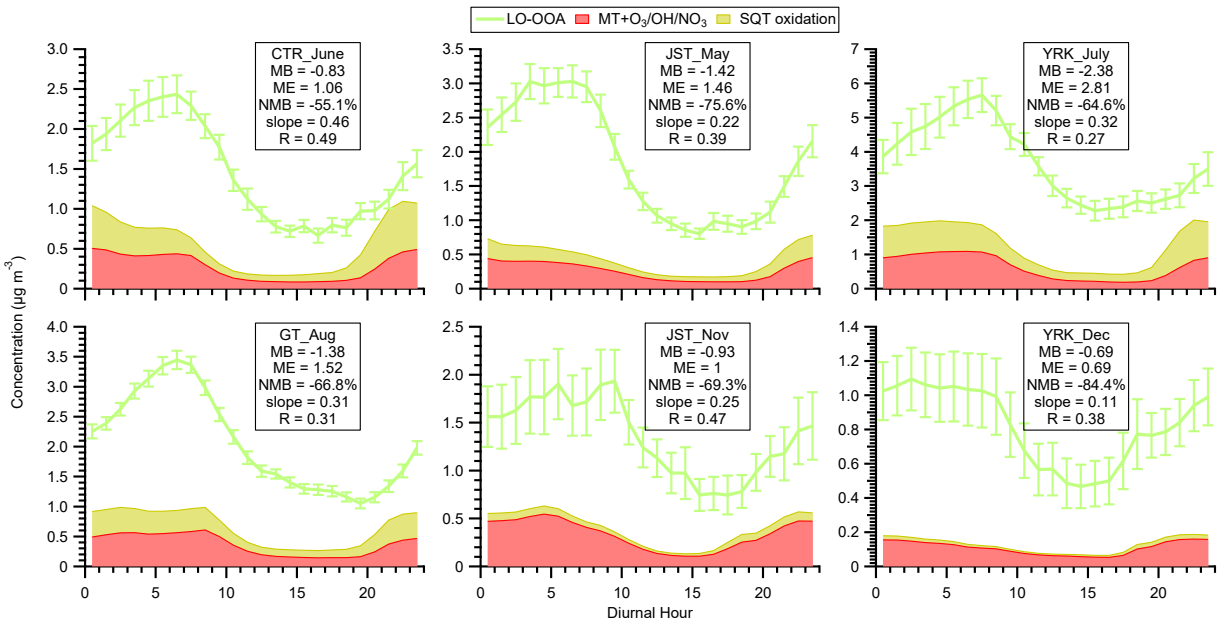

1034

1035 Fig. S20. The diurnal trends of LO-OOA and modeled SOA from monoterpenes and
1036 sesquiterpenes at different sampling sites in the southeastern U.S. in the default simulation. The
1037 mean bias (MB), mean error (ME), and normalized mean bias (NMB) are shown for each site. The
1038 slopes and R are obtained by least square fit.

1039

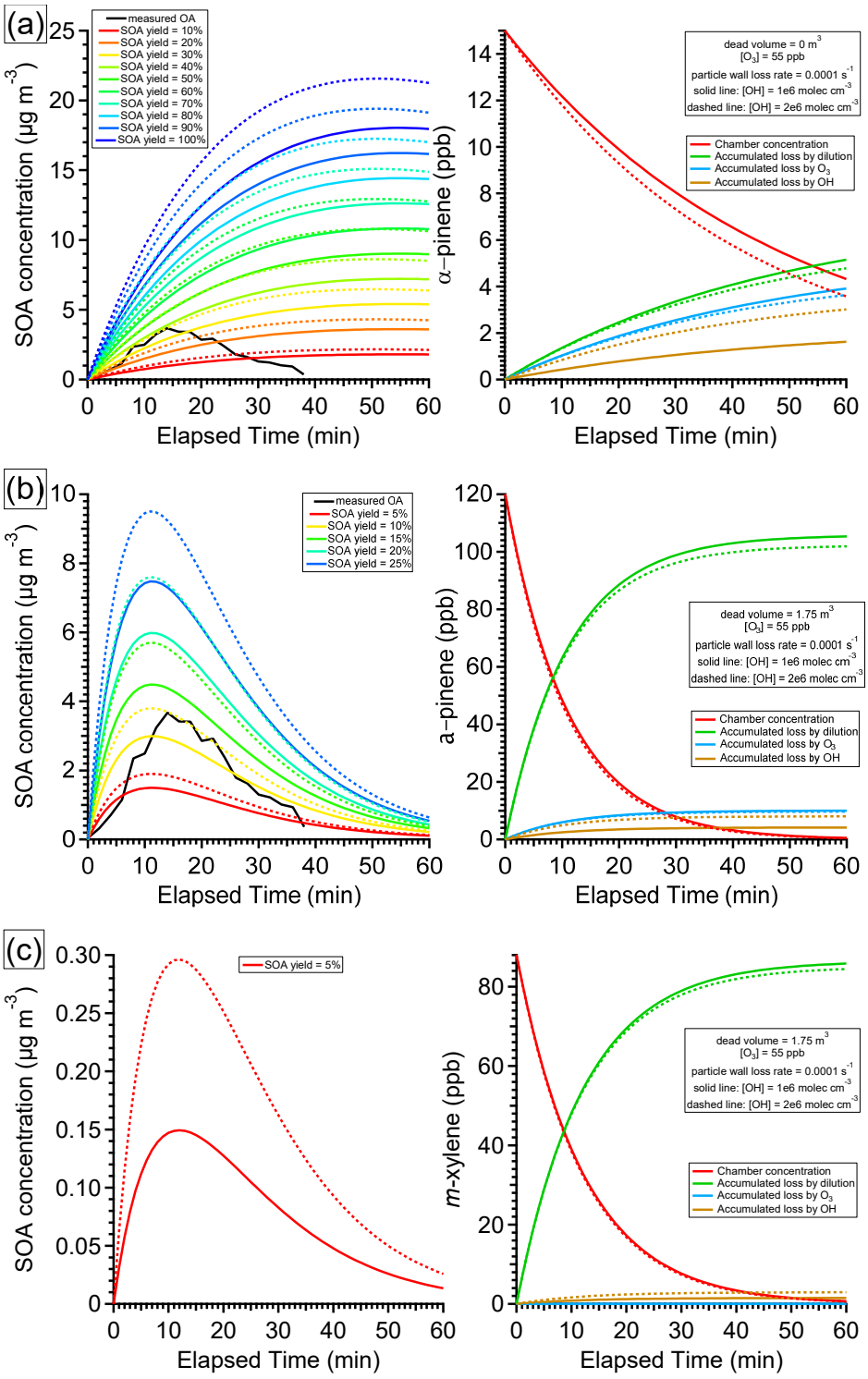

Fig. S21. Simulated time series of VOCs and SOA based on a simple box model. (a) α-pinene experiments assuming a range of SOA yields and no dead volume. (b) α-pinene experiments assuming a range of SOA yields and 1.75 m^3 dead volume. (c) *m*-xylene experiments assuming 5% SOA yield and 1.75 m^3 dead volume.

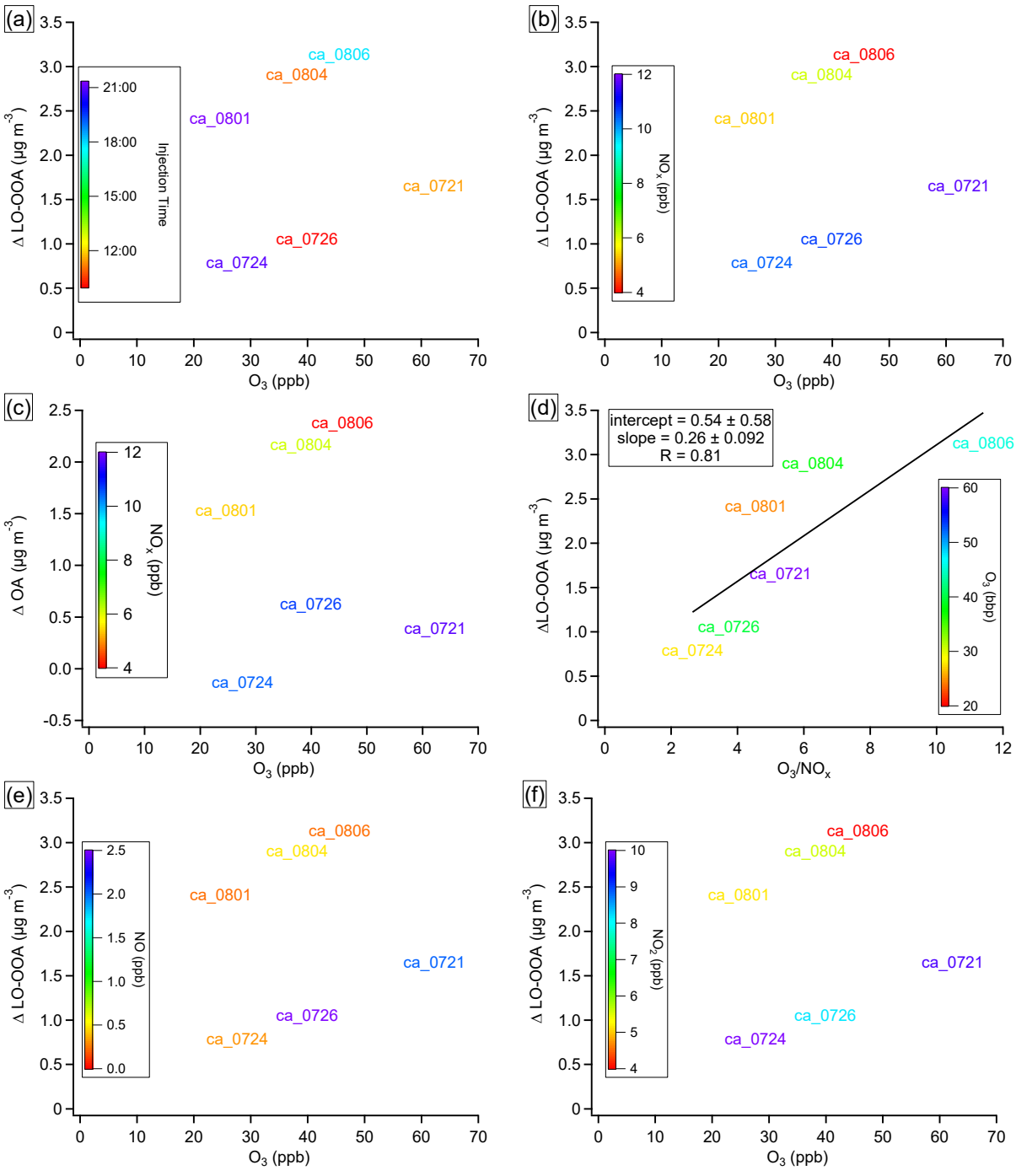

Fig. S22. The influence of NO_x on β-caryophyllene SOA formation. (a) ΔLO-OOA as a function of O_3, colored by injection time. (b) ΔLO-OOA as a function of O_3, colored by NO_x. (c) ΔOA as a function of O_3, colored by injection time. (d) ΔLO-OOA as a function of O_3/NO_x ratio, colored by O_3. The slopes and intercepts are obtained by least square fit. (e) ΔLO-OOA as a function of O_3, colored by NO. (f) ΔLO-OOA as a function of O_3, colored by NO_2.

Table S1. Sampling sites and periods for the Southeastern Center for Air Pollution and Epidemiology (SCAPE) study and the Southern Oxidant and Aerosol Study (SOAS).

Site (Abbreviation)	Sampling Period
Jefferson Street (JST_May)	5/10/2012 - 6/2/2012
Yorkville (YRK_July)	6/26/2012 - 7/20/2012
Georgia Tech (GT_Aug)	7/20/2012 - 9/4/2012
Jefferson Street (JST_Nov)	11/6/2012 - 12/4/2012
Yorkville (YRK_Dec)	12/5/2012 - 1/10/2013
Centreville (CTR_June)	6/1/2013 – 7/15/2013

Table S2. The experimental conditions of laboratory α-pinene experiments.

Expt.	$[HC]_0$ (ppb)	Oxidant precursor	RH	NO (ppb)[b]	NO_2 (ppb)[b]	O_3 (ppb)[b]	OH (10^6 molec cm^{-3})[e]
1	334[a]	H_2O_2	40%	<DL, <DL[c]	<1, <1[c]	N.A.	1.0
2	174[a]	HONO	<5%	269, 167	310, 440	5, 32	10.9
3	15	NO_2	50%	23, 7[d]	60, 60	20, 71	3.6

[a]More than 100ppb α-pinene is injected in the first two experiments. It is because these two experiments were designed to produce large amounts of SOA for filter collection and offline analysis.

[b]There are two values in these columns. The first value represents the initial concentration when turning on the lights. The second value represents the concentration when the OA concentration reaches about 10 μg m^{-3}.

[c]Background NO_x level in the chamber.

[d]The initial concentrations of NO, NO_2, and O_3 in NO_2+hν experiments are reported at 3 min after turning on lights.

[e]The OH concentration is estimated based on the decay of α-pinene, after considering the consumption of α-pinene by O_3.

Table S3. The properties of the lumped oxidation products from monoterpenes + O_3/OH.

Species	α[1]	C*[1]	enthalpy[1]	Potential surrogate structure	nC[2]	nO[2]	nH[2]	MW	OM/OC	H[3]	V lebas	Dg	density
	g g^{-1}	µg m^{-3}	kJ mol^{-1}					g mol^{-1}	g g^{-1}	M atm^{-1}	cm^3 mol^{-1}	cm^2 s^{-1}	g cm^{-3}
MT1	0.040	0.01	102.0	$C_{15}H_{24}O_6$ (Zhang et al., 2015)	15	6	24	300	1.67	7.1E+11	355.2	0.0424	1.4
MT2	0.032	0.1	91.0	$C_{10}H_{16}O_4$ (Chan et al., 2009; Zhang et al., 2015)	10	4	16	200	1.67	8.9E+10	236.8	0.0556	1.4
MT3	0.032	1	80.0	pinic acid (Yu et al., 1999)	9	4	14	186	1.72	1.1E+10	214.6	0.0583	1.4
MT4	0.103	10	69.0	hydroxypinonaldehyde (Yu et al., 1999)	10	3	16	184	1.53	1.4E+09	229.4	0.0587	1.4
MT5	0.143	100	58.0	norpinonic acid (Yu et al., 1999)	9	3	14	170	1.57	1.8E+08	207.2	0.0619	1.4
MT6	0.285	1000	47.0	pinonaldehyde (Yu et al., 1999)	10	2	16	168	1.40	2.2E+07	222.0	0.0624	1.4
MT7	0.160	10000	36.0	norpinonaldehyde (Yu et al., 1999)	9	2	14	154	1.43	2.8E+06	199.8	0.0661	1.4

[1]α, C* (@298K), and enthalpies are based on TD fit in Table 1 Saha and Grieshop (2016) assuming an OA concentration of 445 µg m^{-3}.

[2]Number of oxygen per surrogate is based on Donahue et al. (2011) relationship as used in Pye et al. (2017). Number of carbon and oxygen used to find potential surrogate structure.

[3]Henry's Law Coefficients (H) is based on Hodzic et al. (2014) and relationship with C*. An enthalpy of solvation of 50 kJ mol^{-1} is used.

Table S4. Experimental conditions for ambient perturbation experiments.

Perturbation	Expt ID[a]	Date	Injection Time	Perturbation Amount[b]	NO[c] (ppb)	NO_2[c] (ppb)	O_3[c] (ppb)
α-pinene	ap_0718_1	7/18/2016	11:18	14	0.69	3.57	48.3
	ap_0718_2	7/18/2016	21:44	14	0.29	10.12	40.2
	ap_0719_1	7/19/2016	9:48	14	7.98	19.96	31.9
	ap_0719_2	7/19/2016	13:44	14	0.46	4.14	71.6
	ap_0719_3	7/19/2016	17:18	14	0.19	4.29	81.9
	ap_0720_1	7/20/2016	10:52	14	1.96	9.09	56.5
	ap_0720_2	7/20/2016	19:36	14	0.10	3.54	75.0
	ap_0728_1	7/28/2016	10:04	14	1.53	3.97	25.3
	ap_0728_2	7/28/2016	15:40	14	0.75	3.12	32.7
	ap_0729_1	7/29/2016	11:04	14	1.55	5.69	36.8
	ap_0729_2	7/29/2016	16:22	14	0.63	3.61	43.6
	ap_0731	7/31/2016	12:18	14	0.19	2.73	48.5
	ap_0801_1	8/1/2016	12:42	14	0.24	5.28	53.1
	ap_0801_2	8/1/2016	17:06	14	0.25	3.23	44.9
	ap_0802	8/2/2016	13:08	14	0.23	3.41	48.5
	ap_0803	8/3/2016	17:22	14	0.14	2.65	53.2
	ap_0804	8/4/2016	15:18	14	0.27	6.04	53.2
	ap_0805_1	8/5/2016	13:14	14	0.27	6.02	60.5
	ap_0805_2	8/5/2016	17:42	28	0.13	3.13	52.4
β-caryophyllene	ca_0721	7/21/2016	11:32	10	2.02	9.73	62.3
	ca_0724	7/24/2016	20:58	10	0.32	10.12	27.6
	ca_0726	7/26/2016	9:58	10	2.48	8.19	39.9
	ca_0801	8/1/2016	21:20	10	0.24	5.19	24.7
	ca_0804	8/4/2016	11:02	10	0.48	5.60	38.1
	ca_0806	8/6/2016	17:54	10	0.23	3.77	45.6

[a]Expt ID is named as "perturbation species + date + experiment number". For example, ap_0801_1 represents the first α-pinene perturbation experiment on 08/01.

[b]The unit for the perturbation in α-pinene and β-caryophyllene experiments is ppb. The perturbation amounts of α-pinene and β-caryophyllene are estimated based on the VOC injection volume and chamber volume. The amount of VOC injected is not the same as the amounts consumed by oxidants (section S6).

[c]Average concentration during the Chamber_Af period.

Table S5. Sampling periods for the measurements at the GT site from 2012 to 2016.

Year	Sampling Period	Note	Reference
2012	7/21 - 9/3	Continuously ambient measurements	Xu et al. 2015 ACP
2013	8/1/- 8/25	AMS alternates between ambient line and PILS line	Xu et al. 2017 ES&T
2015	8/1 - 8/16	Ambient perturbation experiments and experiments for other purposes	This study
2016	7/1 - 8/6	Ambient perturbation experiments	This study